

Nonlocal form factor of chromomagnetic penguin in $B \rightarrow K \ell^+ \ell^-$ from QCD light-cone sum rules

T. Hurth¹, A. Khodjamirian^{2,3,4,5},
D. Mishra³, Y. Monceaux³, S. Neshatpour³

¹ *PRISMA+ Cluster of Excellence and Institute for Physics (THEP), Johannes Gutenberg University, D-55099 Mainz, Germany*

² *Center for Particle Physics (CPPS), Theoretische Physik 1, Universität Siegen, D-57068 Siegen, Germany*

³ *Université Claude Bernard Lyon 1, CNRS/IN2P3, Institut de Physique des 2 Infinis de Lyon, UMR 5822, F-69622, Villeurbanne, France*

⁴ *Theoretical Physics Department, CERN, CH-1211 Geneva 23, Switzerland*

⁵ *Institut Universitaire de France (IUF), 75005 Paris, France*

Abstract

The branching fraction of the $B \rightarrow K \ell^+ \ell^-$ decay has been measured recently by the LHC experiments, showing a deviation from theory predictions based on the Standard Model (SM). A major challenge in achieving a complete SM prediction and interpreting this discrepancy lies in the treatment of nonlocal hadronic effects. In $B \rightarrow K \ell^+ \ell^-$, these effects are cast in a single nonlocal form factor, a function of squared momentum transfer q^2 to the lepton pair. One of the previously used methods provides this form factor in the region of spacelike momentum transfer, $q^2 < 0$, matching the result to the hadronic dispersion relation, which is then continued to the physical region. The calculation done so far was a combination of QCD factorisation for hard-gluon contributions with light-cone sum rules (LCSRs) for soft-gluon ones. In this work, we calculate for the first time the complete nonlocal form factor at $q^2 < 0$ for one of the effective operators, the chromomagnetic operator O_{8g} , applying the method of LCSRs with B -meson distribution amplitudes. We compute, both analytically and numerically, the operator-product expansion (OPE) diagrams with hard-gluon exchanges, analyse their structure and hierarchy, and obtain their spectral density entering the LCSR together with soft-gluon contributions. This study paves the way for our next task, a complete calculation of nonlocal $B \rightarrow K \ell^+ \ell^-$ form factor at spacelike q^2 , including the dominant contributions of current-current operators, known as charm-loops.

Contents

1	Introduction	3
2	Nonlocal form factor of the operator O_{8g}	4
3	Light-cone sum rule for the nonlocal form factor	5
4	Computation of OPE diagrams	7
4.1	Nomenclature of diagrams	7
4.2	Form-factor-like diagrams	10
4.3	Hard-scattering diagrams	13
4.4	Soft-gluon diagrams	14
4.5	Power counting	15
5	Numerical Results	16
6	Conclusion and outlook	20
A	Notations and conventions	22
B	B-meson distribution amplitudes	22
C	Imaginary parts of different functions	24
D	Expressions for invariant functions	24
D.1	Form-factor-like contributions	24
D.2	Hard-scattering contributions	27
D.3	Soft-gluon contribution	29
E	Coefficients in the LCSR integrals	30
E.1	Coefficients $\tilde{B}_i^{(j,\phi/\Phi)}$	30
E.2	Coefficients $D_i^{(j,\phi/\Phi)}$	31
E.3	Coefficients $F_n^{(X)}$	34

1 Introduction

Exclusive flavour-changing neutral-current (FCNC) decays of B -meson are facing a long-standing tension between theory and experiment. Currently, the most striking is the situation with the simplest observable—the branching fraction of the $B \rightarrow K\ell^+\ell^-$ decay. The recent measurement of the CMS collaboration [1] reveals a good agreement with the earlier LHCb data [2] on this process. If one takes the most “theoretically clean” bin $1.1 \text{ GeV}^2 < q^2 < 6.0 \text{ GeV}^2$ of the momentum transfer q to the lepton pair, the average of these two measurements lies below theory predictions based on the Standard Model (SM), with a tension in the range of 1.7σ – 4.1σ , depending on the choice of local form factors (see e.g., a recent detailed comparison presented in [3]).

In SM, the $B \rightarrow K\ell^+\ell^-$ decay amplitude, being relatively simple kinematically, involves a nontrivial QCD dynamics embedded in two contributions of different origin. The dominant part of the decay amplitude is determined by the effective local operators $O_{9,10}$ and O_7 . The $B \rightarrow K$ hadronic matrix elements of these operators are reduced to local form factors that are accurately calculated: (i) in lattice QCD at large q^2 and (ii) from QCD light-cone sum rules (LCSRs) in the kinematically enhanced low- q^2 region. The remaining, presumably subdominant part of the $B \rightarrow K\ell^+\ell^-$ decay amplitude represents a complicated superposition of various long-distance nonlocal effects, expressed in the form of a single invariant function, the nonlocal form factor. Currently, for all FCNC exclusive B decays, the main stumbling blocks limiting their precision analysis are these nonlocal form factors.

In the exclusive $b \rightarrow s\ell^+\ell^-$ decays, these effects are generated by an overlap of the weak $b \rightarrow s\bar{q}q$ transition (where $q = u, d, s, c$) with the electromagnetic (e.m.) emission of a lepton pair. The dominant contribution, involving the $b \rightarrow s\bar{c}c$ transition, is known as a charm-loop effect. In lattice QCD, dedicated investigations of nonlocal effects in $B \rightarrow K\ell^+\ell^-$ decays started only recently (see e.g., [4]). The existing QCD-based calculations of these effects are mainly based on the heavy b -quark mass limit and on heavy-quark effective theory (HQET).

The first systematic approach [5] to nonlocal effects in $B \rightarrow K^{(*)}\ell\ell$ was using the QCD factorisation (QCDF) in terms of the light-cone distribution amplitudes of B -meson (in HQET) and $K^{(*)}$ meson. The resulting factorisation formula, derived on the basis of this approach, includes, in addition to the leading-order charm-loop, also the effects of hard-gluon exchanges. Applying QCDF in the physical region of the $B \rightarrow K^{(*)}\ell^+\ell^-$ decay, e.g. for the bin $1.1 < q^2 < 6.0 \text{ GeV}^2$, one has to assume, first of all, that a quark-level calculation of the charm-loop is directly applicable in the timelike region. Also, by now QCDF cannot be extended to subleading powers in the heavy mass scale. In particular, the soft-gluon effects generating such power corrections to the factorisation formulas are not yet accessible.

In [6], a different approach was developed, shifting the calculation of nonlocal form factors into the region of spacelike values of q^2 , far below hadronic thresholds. This enables to safely compute the contributions of soft gluons emitted by the charm-loop, applying LCSRs with B -meson distribution amplitudes (DAs). The other new element of this approach is the extensive use of the hadronic dispersion relation in the variable q^2 for a nonlocal form factor. Matching the parameters of this relation to the calculated form factor at spacelike q^2 , one then continues the latter in the form of a dispersion relation into the physical region of q^2 , avoiding a direct use of quark-level expressions in the timelike region. The price for that is an inevitable dependence of the result on the chosen ansatz for the resonances structure of the dispersion relation.

Following this approach, a complete calculation of nonlocal form factor for $B \rightarrow K\ell^+\ell^-$ was accomplished in [7] (see also [8]). The contributions of all effective operators and all quark topologies were included, combining QCDF for the perturbative contributions with LCSRs for the $B \rightarrow K$ form factors and for the soft-gluon contributions. In [9–11], this

method was extended to the $B \rightarrow K^* \ell^+ \ell^-$ mode and further developed, adding dispersive bounds.

Facing a noticeable discrepancy between the predicted and measured $B \rightarrow K \ell^+ \ell^-$ branching fractions, it is timely to carefully revise the methods used to evaluate nonlocal effects. In particular, it is desirable to reanalyse the approach mentioned above that combines LCSR and QCDF at spacelike q^2 with hadronic dispersion relation in the physical region. Before turning to the phenomenological component of that approach, which is mainly the dispersion relation, it is necessary to upgrade the QCD-based component. To this end, we plan to undertake a systematic computation of all contributions to the $B \rightarrow K \ell^+ \ell^-$ nonlocal form factor at spacelike q^2 within one and the same LCSR method and with a uniform nonperturbative input in a form of B -meson DAs. This program is, however, technically very demanding, mainly because the operator-product expansion (OPE) of the underlying correlation function used for LCSR contains two-loop diagrams with several mass scales.

The aim of this paper is to accomplish the first step in this direction and to prove that our program is feasible for a selected contribution to the $B \rightarrow K \ell^+ \ell^-$ nonlocal form factor. To this end, we choose the chromomagnetic operator O_{8g} which does not contain any additional energy/mass scale, such as c -quark mass inherent for the charm-loop. With this choice, we avoid too complicated two-loop diagrams related to the hard-gluon exchanges between the charm-loop and other quarks in that process. On the other hand, calculating the nonlocal form factor for O_{8g} is a convenient starting point because we will reveal the relative importance of separate diagrams depending on their topology and on the location of the virtual photon emission point. We will also reproduce properties of the nonlocal form factor, such as the imaginary part emerging already at $q^2 < 0$.

The paper is organised as follows. In Section 2, we introduce the nonlocal form factor for $B \rightarrow K \ell^+ \ell^-$ associated with the chromomagnetic operator O_{8g} . Section 3 presents the derivation of the corresponding LCSRs for this nonlocal form factor. In Section 4, we describe the computation of the OPE diagrams, beginning with the nomenclature of diagrams and proceeding through the hard-factorisable, hard nonfactorisable, and soft nonfactorisable topologies, followed by the discussion on power counting. Section 5 contains the numerical analysis of our results, and Section 6 provides a summary of the main findings and an outline of the future plans.

2 Nonlocal form factor of the operator O_{8g}

In the SM, the effective Hamiltonian of the $b \rightarrow s$ transitions contains, among other operators, also the chromomagnetic operator O_{8g} with its Wilson coefficient C_{8g} . This local, dimension-six operator emerges after integrating out virtual t -quarks and W -bosons in the loop diagrams where a single gluon is emitted. We use the standard form:

$$O_{8g} = -\frac{g_s}{16\pi^2} m_b \bar{s} \sigma^{\mu\nu} P_R G_{\mu\nu} b, \quad (2.1)$$

where $P_R \equiv (1 + \gamma_5)/2$ and the suppressed part proportional to m_s is neglected (the convention used for $\sigma^{\mu\nu}$ is given in Appendix A).

We aim at calculating the matrix element in which a time-ordered product of the operator O_{8g} with the quark e.m. current

$$j_\mu^{em} = \sum_{q=u,d,s,c,b} Q_q \bar{q} \gamma_\mu q, \quad (2.2)$$

is sandwiched between the B -meson and kaon on-shell states:

$$\begin{aligned}\mathcal{H}_\mu^{(BK, O_{8g})}(p, q) &= i \int d^4x e^{iq \cdot x} \langle \bar{K}(p) | T \{ j_\mu^{\text{em}}(x), C_{8g} O_{8g}(0) \} | \bar{B}(p_B) \rangle \\ &= ((p \cdot q) q^\mu - q^2 p_\mu) \mathcal{H}^{(BK, O_8)}(q^2),\end{aligned}\quad (2.3)$$

where the four-momentum transfer is $q = p_B - p$ and the B -meson and kaon momenta are on-shell, $p_B^2 = m_B^2$, $p^2 = m_K^2$. In the r.h.s. of (2.3), we use the e.m. current conservation, allowing us to reduce this hadronic matrix element to a single invariant function of the momentum transfer squared, that is the nonlocal form factor denoted as $\mathcal{H}^{(BK, O_8)}(q^2)$.

Since we are not considering the full $B \rightarrow K \ell^+ \ell^-$ decay amplitude in this paper, and, in particular, we ignore the ‘‘direct’’ operators O_9, O_{10} and O_7 , it is more convenient to treat the matrix element (2.3) as a part of the $B \rightarrow K \gamma^*$ amplitude with a virtual photon emission. This interpretation also makes it easier to consider the spacelike region of momentum transfer, $q^2 < 0$ which is unphysical for the decay into a lepton pair, but plays a major role here, being accessible with our calculational method.

The amplitude (2.3) with the operator O_{8g} plays a minor role compared to the dominant nonlocal effects in $B \rightarrow K \gamma^*$ transitions, stemming from the intermediate c -quark loop. These ‘‘charm-loop’’ effects emerge due to the $b \rightarrow c \bar{c} s$ operators $O_{1,2}^{(c)}$ in the effective Hamiltonian with their Wilson coefficients $C_{1,2}$ larger than C_{8g} . Still, the coefficient of the chromomagnetic operator itself is much larger than Wilson coefficients of the quark-penguin or electroweak-penguin operators, which we neglect hereafter.¹

To quantify the O_{8g} effect in the total budget of nonlocal contributions to $B \rightarrow K \gamma^*$, we introduce the ratio of this effect to the leading-order charm-loop with a virtual photon emission, taken in the factorisable approximation. Using the expression for the latter from [7], we define

$$R_{(O_8/O_{1,2}^c)}(q^2) \equiv \frac{\mathcal{H}^{(BK, O_8)}(q^2)}{\mathcal{H}^{(BK, O_{1,2}^c)}(q^2)}, \quad (2.4)$$

where

$$\mathcal{H}^{(BK, O_{1,2}^c)}(q^2) = \frac{Q_c}{8\pi^2} \left(\frac{C_1}{3} + C_2 \right) g(m_c^2, q^2) f_{BK}^+(q^2), \quad (2.5)$$

and

$$g(m_c^2, q^2) = - \left(\ln \frac{m_c^2}{\mu^2} + 1 \right) + q^2 \int_{4m_c^2}^{+\infty} ds \frac{\sqrt{1 - \frac{4m_c^2}{s}} \left(1 + \frac{2m_c^2}{s} \right)}{s(s - q^2)}, \quad (2.6)$$

is the well-known loop function, μ is the renormalisation scale and $f_{BK}^+(q^2)$ is the $B \rightarrow K$ local form factor of the vector $b \rightarrow s$ current.

3 Light-cone sum rule for the nonlocal form factor

We use the method of LCSRs with B -meson DAs in HQET, that was initially developed in [12] (also in the framework of soft-collinear effective theory (SCET) in [13]), to obtain the

¹Hence, we also neglect the mixing effects between operators for simplicity.

$B \rightarrow$ light meson form factors, including also the $B \rightarrow K$ local form factors (see [14] for a detailed review of more recent results). Following [7], we start from the correlation function:

$$\begin{aligned}\Pi_{\nu\mu}(p, q) &= i^2 \int d^4y e^{ip\cdot y} \int d^4x e^{iq\cdot x} \langle 0 | T \{ j_{5\nu}^K(y) j_\mu^{\text{em}}(x) C_{8g} O_{8g}(0) \} | \bar{B}(p_B) \rangle \\ &= i p_\nu q_\mu \Pi(p^2, q^2) + \dots, \end{aligned} \quad (3.1)$$

where we select a single kinematical structure from the Lorentz-expansion, so that the invariant amplitude $\Pi(p^2, q^2)$ will be used in the resulting LCSR. The other structures are irrelevant and denoted by ellipsis. In the correlation function of our choice the kaon is interpolated by the axial current,

$$j_{5\nu}^K(x) = \bar{q}(x) \gamma_\nu \gamma_5 s(x), \quad (3.2)$$

with $q = u, d$ for the charged and neutral kaon, respectively.

Considering the correlation function (3.1) as an analytic function of the variable p^2 at fixed spacelike q^2 , we derive a dispersion relation in the kaon channel. To this end, we apply unitarity condition, inserting in (3.1) a complete set of intermediate hadronic states carrying kaon quantum numbers. Isolating the kaon pole, we have:

$$\Pi_{\nu\mu}(p, q) = \frac{\langle 0 | j_{5\nu}^K | \bar{K}(p) \rangle i \int d^4x e^{iq\cdot x} \langle \bar{K}(p) | T \{ j_\mu^{\text{em}}(x) C_{8g} O_{8g}(0) \} | \bar{B}(p_B) \rangle}{m_K^2 - p^2} + \int_{s_h}^{\infty} ds \frac{\rho_{\nu\mu}^h(s, p, q)}{s - p^2}, \quad (3.3)$$

where the spectral density $\rho_{\nu\mu}^h(s, p, q) = i p_\nu q_\mu \rho^h(s, q^2) + \dots$, in which we isolate the relevant invariant function, is formed by the sum over contributions of all heavier than kaon hadronic states with the quantum numbers of the $j_{5\nu}^K$ current. The lightest in this sum is the $K\pi\pi$ continuum state, hence $s_h = (m_K + 2m_\pi)^2$. Applying the standard definition for the decay constant of the kaon:

$$\langle 0 | j_{5\nu}^K | \bar{K}(p) \rangle = i f_K p_\nu, \quad (3.4)$$

and the definition (2.3) of the nonlocal form factor, we obtain from (3.3) the dispersion relation for the invariant amplitude:

$$\Pi(p^2, q^2) = \frac{f_K(m_B^2 - q^2 - m_K^2) \mathcal{H}^{(BK, O_8)}(q^2)}{2(m_K^2 - p^2)} + \int_{s_h}^{\infty} ds \frac{\rho^h(s, q^2)}{s - p^2}, \quad (3.5)$$

where we replace $p^2 \rightarrow m_K^2$ in the kinematical factor $(p \cdot q)$ to remove the constant term that will vanish after Borel transform.

In the following section, we compute the correlation function (3.1) applying the light-cone OPE in terms of B -meson distribution amplitudes. In the OPE result, we isolate the relevant invariant amplitude:

$$\Pi_{\nu\mu}^{(\text{OPE})}(p, q) = i p_\nu q_\mu \Pi^{(\text{OPE})}(p^2, q^2) + \dots,$$

transforming it to the form of a dispersion integral in the variable p^2 :

$$\Pi^{(\text{OPE})}(p^2, q^2) = \frac{1}{\pi} \int_{m_s^2}^{\infty} ds \frac{\text{Im} \Pi^{(\text{OPE})}(s, q^2)}{s - p^2}. \quad (3.6)$$

In the spacelike p^2 -region of the OPE validity, we equate the dispersion relation (3.5) to the amplitude $\Pi^{(\text{OPE})}(p^2, q^2)$. The dispersion form of the latter amplitude allows us to apply the usual quark-hadron duality approximation for the integral over the heavier state in the dispersion relation (3.5):

$$\int_{s_h}^{\infty} ds \frac{\rho^h(s, q^2)}{s - p^2} = \frac{1}{\pi} \int_{s_0}^{\infty} ds \frac{\text{Im} \Pi^{(\text{OPE})}(s, q^2)}{s - p^2}, \quad (3.7)$$

where s_0 is the effective threshold. After that, we substitute (3.6) to the l.h.s. of (3.5) and replace the integral over $\rho^h(s)$ by the duality approximation (3.7). After subtracting equal integrals from both parts of the resulting equation and after a standard Borel transform, we obtain the desired LCSR for the nonlocal form factor:

$$\mathcal{H}^{(BK, O_8)}(q^2) = \frac{2 e^{m_K^2/M^2}}{f_K (m_B^2 - m_K^2 - q^2)} \frac{1}{\pi} \int_{m_s^2}^{s_0} ds e^{-s/M^2} \text{Im} \Pi^{(\text{OPE})}(s, q^2). \quad (3.8)$$

This sum rule was earlier derived also in [7] but the OPE calculated there was limited to a single specific contribution due to the soft-gluon absorbed in three-particle DAs of B -meson. The most important parts with hard-gluon were estimated using QCDf results. In what follows, we will accomplish, for the first time the complete computation of OPE including both hard-gluon and soft-gluon parts within one and the same method.

4 Computation of OPE diagrams

4.1 Nomenclature of diagrams

In Fig. 1, the diagrams corresponding to the OPE of the correlation function (3.1) are depicted. For perturbative gluons, we confine ourselves to the leading-order, $O(\alpha_s)$ accuracy, so that they are emitted from the operator O_{8g} and absorbed by one of the three quark lines. Altogether, there are three sets of one-loop diagrams denoted by (A), (B) and (C). Each set is characterised by a definite quark-gluon topology, and contains four separate diagrams corresponding to four possible ways to insert the e.m. current, or, in other words, to emit a virtual photon from quark lines. For the sake of compactness, we show in a single subfigure all four diagrams of the same topology, numbering them according to the e.m. current insertion point, counted clockwise. For instance, (A1) is the diagram of type A where the e.m. current is inserted in the virtual b -quark line.

The diagrams (A), (B), (C) with hard gluon exchanges are described by convolutions of the short-distance perturbative kernels with the two-particle, quark-antiquark B -meson DAs. In these DAs, we take into account the leading and subleading twist-2 and twist-3 components. Here we follow the twist expansion of the B -meson DAs worked out in [15].

The gluon emitted from the O_{8g} operator vertex in the correlation function can also have a low virtuality of $O(\Lambda_{QCD}^2)$. Such a “soft” gluon, together with the heavy-light quark-antiquark pair, forms B -meson three-particle DAs. There are three soft-gluon diagrams as indicated in the subfigure (D) of Fig. 1. They correspond to the three possible ways to insert the e.m. current. In the OPE, the three-particle DAs start from twist-3. That will be our default choice, consistent with the adopted twist-3 accuracy of the two-particle DAs. To investigate the sensitivity to higher twists, we will also include into the soft-gluon part of the correlation function all three-particle DAs up to twist-6. Note that in these diagrams, both the gluon and quark entering the B -meson DA are emitted from a single point, making

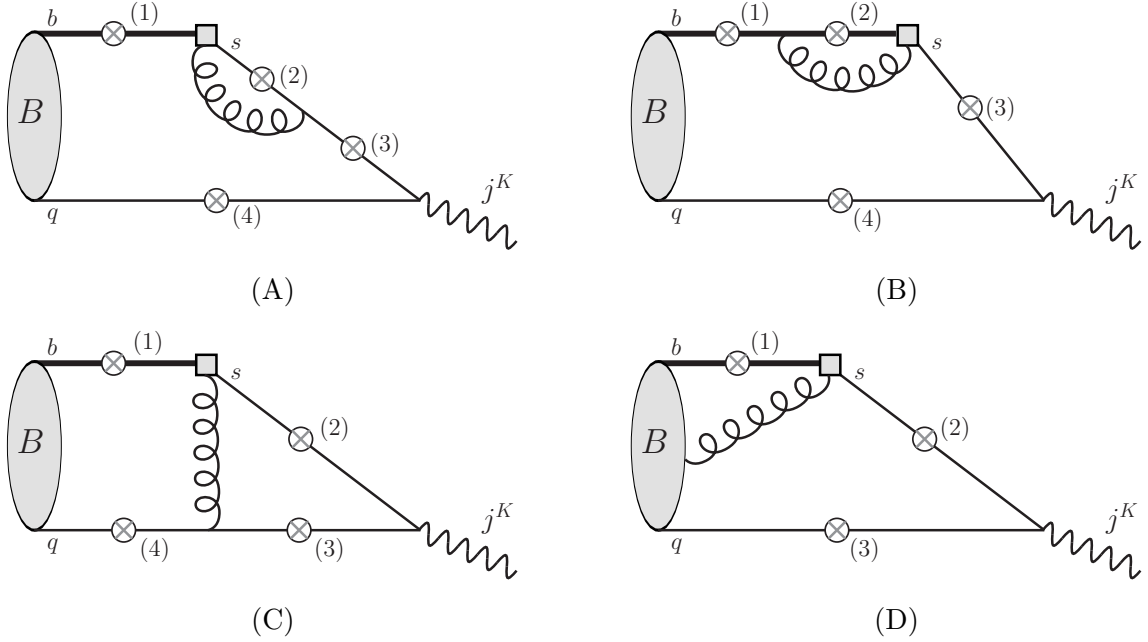


Figure 1: Diagrams for the correlation function (3.1). The chromomagnetic operator O_{sg} is denoted by a shaded square, the B -meson DAs are shown with a shaded blob. The circled crosses indicate possible emission points of a virtual photon.

the light-cone expansion with respect to this emission automatically local, and leaving only one interval x^2 which has to be close to the light-cone. One of the advantages of the LCSR method is that the complete correlation function can be separated into a short-distance perturbative part and a long-distance part represented by B -meson DAs. This factorisation property is valid for each diagram in Fig. 1 including hard-gluon and soft-gluon contributions. In this paper we do not go further into more detail in that direction, and will not dwell on the renormalisation effects and separation-scale dependence.

In the QCdf approach [5] to $B \rightarrow K \ell^+ \ell^-$ decay, if we only retain the O_{sg} operator, there are two distinct types of diagrams. One is represented by perturbative gluon exchanges adjacent to the operator vertex, so that the long-distance part can be reduced to a local $B \rightarrow K$ form factor. The other type of diagrams contains hard-scattering, that is, the exchange of perturbative gluon between the operator vertex and spectator quark in B -meson. We note that some of the diagrams in Fig. 1 have their counterpart in QCdf, if we, conditionally, replace the kaon interpolating current by the kaon DA. In particular, diagrams (A1)–(A3), (B1)–(B3) can be reduced to the local form factors, whereas diagrams (C1)–(C4) can be classified as hard-scattering ones. However, diagrams (A4) and (B4), where the virtual photon is emitted from the spectator quark, with no gluon exchange between quarks, have no analogs among the QCdf contributions. In fact, we shall see that in our LCSR these two diagrams, as well as diagram (D3) do not contribute, for the reason to be explained in detail below. Furthermore, diagrams (D1)–(D3) with soft gluons are also absent in the present calculations based on QCdf, because in that method a factorisation formula at subleading power is not established yet.

Accordingly, in what follows, we will separate from each other, the form factor-like, hard-scattering and soft contributions to the LCSR (3.8), stemming, respectively, from the diagrams $\{(A1)–(A3), (B1)–(B3)\}$, $\{(C1)–(C4)\}$ and $\{(D1)–(D2)\}$. In addition, in each of these three parts we will also collect contributions in which a virtual photon is emitted from a quark line with a certain flavour, in our case b, s or $q = u, d$. These flavour-specific contributions will be distinguished by their global quark-charge factor Q_b, Q_s or $Q_{u,d}$, respectively,

The task to evaluate the OPE diagrams is somewhat simplified by the fact that only the imaginary part of the invariant amplitude $\Pi(p^2, q^2)$ in the variable p^2 contributes to the LCSR (3.8). A direct computation, to be discussed in detail in the following subsections, reveals that the diagrams (A4), (B4) and (D3) develop imaginary part at large $p^2 = s$, far above a typical duality interval $s < s_0 \sim O(1 \text{ GeV}^2)$ for the kaon, hence, these three diagrams do not contribute to the LCSR.

The shift of imaginary part has in fact a qualitative explanation based on kinematics². Taking the imaginary part of the diagrams (A4), (B4), (D3) in the variable p^2 , we put on-shell the intermediate light-quark line between the kaon and e.m. current vertices. The s -quark line in these diagrams remains off-shell, because it absorbs the initial momentum p_b of the quasi-on-shell b -quark line in the B -meson (or the sum of b -quark and soft gluon momenta in the diagram (D3)). The fact that there is an intermediate quark-gluon loop in the diagrams (A4), (B4) does not play a role, if only kinematics is concerned. In the rest frame of the B -meson, $p_B = (m_B, \vec{0})$, we have two pairs of back-to-back three-momenta: first, $\vec{p}_b = -\vec{p}_q$ for the B -meson constituents and second, $\vec{p} = -\vec{q}$ for the kaon-interpolating and e.m. currents. Energy-momentum conservation tells that in this frame:

$$|\vec{p}_b| = |\vec{p}_q| = \frac{m_B^2 - m_b^2}{2m_B} \simeq \bar{\Lambda}, \quad |\vec{p}| = |\vec{q}| = \frac{\lambda^{1/2}(m_B^2, q^2, p^2)}{2m_B}, \quad (4.1)$$

where in the first equation the HQET parameter $\bar{\Lambda} = m_B - m_b$ is introduced and terms of $O(\bar{\Lambda}^2)$ are neglected, and in the second equation λ is the Källén function. At the same frame, the four-momentum f of the light-quark line between currents has the following components:

$$f_0 = \frac{m_b^2 - p^2 + q^2}{2m_B}, \quad |\vec{f}| = |\vec{p}_b|^2 - 2|\vec{p}_b||\vec{p}|\cos\theta + |\vec{p}|^2, \quad (4.2)$$

where θ is the angle between \vec{p}_b and \vec{p} . Furthermore, due to (4.1), these components are expressed via invariant variables p^2 and q^2 . Hence, the on-shell condition $f^2 = f_0^2 - \vec{f}^2 = 0$ yields a relation between these variables:

$$q^2 + \frac{\bar{\Lambda}}{m_B} [(m_B^2 - p^2 + q^2)^2 - 4m_B^2 q^2]^{1/2} \cos\theta - O(\bar{\Lambda}^2) = 0. \quad (4.3)$$

This relation can only be satisfied if the variable $p^2 \gtrless O(m_B^2 + (-)q^2)$ at nonzero $\cos\theta > (<)0$. Note that in the region of spacelike $q^2 < 0$, where LCSRs will be used, we have, parametrically, $\Lambda_{QCD}^2 \ll |q^2| \ll m_b^2$. Hence, the corresponding values of p^2 are much larger than m_K^2 , implying that the pole in the $p^2 = s > 0$ region for the diagrams (A4), (B4), (D3) is located far above a typical duality interval for the kaon current.

Taking into account the separation of contributions into form-factor-like (ff), hard scattering (hs) and soft-gluon (sg) as suggested above, the OPE result to be put on r.h.s. of LCSR (3.8) takes the following form

$$\frac{1}{\pi} \int_{m_s^2}^{s_0} ds e^{-s/M^2} \text{Im} \Pi^{(\text{OPE})}(s, q^2) = \mathcal{P}_{(ff)}^{(\text{OPE})}(M^2, q^2) + \mathcal{P}_{(hs)}^{(\text{OPE})}(M^2, q^2) + \mathcal{P}_{(sg)}^{(\text{OPE})}(M^2, q^2), \quad (4.4)$$

where the three terms above are further split into separate diagram contributions, factoring

²A similar consideration for a different QCD sum rule can also be found in [16].

the quark charges for convenience:

$$\begin{aligned} \mathcal{P}_{(ff)}^{(\text{OPE})}(M^2, q^2) = & f_B m_B \left(\frac{\alpha_s C_F}{32\pi} \right) m_b C_{8g} \left\{ Q_b \left[I^{(A1)}(M^2, q^2) + I^{(B1)}(M^2, q^2) + I^{(B2)}(M^2, q^2) \right] \right. \\ & \left. + Q_s \left[I^{(A2)}(M^2, q^2) + I^{(A3)}(M^2, q^2) + I^{(B3)}(M^2, q^2) \right] \right\}, \end{aligned} \quad (4.5)$$

$$\begin{aligned} \mathcal{P}_{(hs)}^{(\text{OPE})}(M^2, q^2) = & f_B m_B \left(\frac{\alpha_s C_F}{32\pi} \right) m_b C_{8g} \left\{ Q_b I^{(C1)}(M^2, q^2) + Q_s I^{(C2)}(M^2, q^2) \right. \\ & \left. + Q_d \left[I^{(C3)}(M^2, q^2) + I^{(C4)}(M^2, q^2) \right] \right\}, \end{aligned} \quad (4.6)$$

$$\mathcal{P}_{(sg)}^{(\text{OPE})}(M^2, q^2) = f_B \frac{m_b}{8\pi^2} C_{8g} \left\{ Q_b I^{(D1)}(M^2, q^2) + Q_s I^{(D2)}(M^2, q^2) \right\}. \quad (4.7)$$

In the following subsections we will discuss the computation of separate diagrams, resulting in the analytic expressions for the integrals $I^{(A1), \dots, (D2)}$ entering (4.5), (4.6) and (4.7).

4.2 Form-factor-like diagrams

Here, we discuss in detail how diagrams (A1)–(A3) and (B1)–(B3) in Fig. 1 are computed. As explained above, their contributions are conditionally identified as “form-factor-like” ones. In these diagrams, the perturbative gluon from the O_{8g} operator forms a loop subgraph, while the B -meson spectator quark remains intact. The soft physics is then entirely encoded in the two-particle B -meson light-cone distribution amplitudes (LCDAs).

As an illustrative example, we describe in more detail the computation of diagram (A1), where the virtual photon is emitted from the b -quark line. The corresponding initial expression, with all quark and gluon fields in the diagram shown explicitly, reads:

$$\begin{aligned} \Pi_{\nu\mu}^{(A1)}(q, p) = & -i^4 \int d^4 y e^{ip \cdot y} \int d^4 x e^{iq \cdot x} \int d^4 z \langle 0 | T \left\{ [\bar{d}\gamma_\nu \gamma_5 s](y), g_s A^\sigma(z) [\bar{s}\gamma_\sigma T^a s](z), \right. \\ & \left. \frac{g_s m_b}{16\pi^2} C_{8g} k^\eta A^\rho(0) T^a [\bar{s}\sigma_{\rho\eta}(1 + \gamma_5)b](0), Q_b [\bar{b}\gamma_\mu b](x) \right\} | B(p_B) \rangle, \end{aligned} \quad (4.8)$$

where, as before, $p_B = p + q$ and $p_B^2 = m_B^2$. Contracting the quark, antiquark and gluon fields into the propagators in accordance with the topology of diagram (A1), we replace the emerging $B \rightarrow$ vacuum matrix element of a bilocal heavy-light quark-antiquark operator by the two-particle B -meson DAs, using the definition (B.1).

The result, integrated over the coordinates then reads:

$$\begin{aligned}
\Pi_{\nu\mu}^{(A1)}(q, p) &= -i f_B m_B \left(\frac{\alpha_s C_F}{32\pi} \right) m_b C_{8g} Q_b \int_0^\infty d\omega \int \frac{d^4 k}{(2\pi)^4} \\
&\times \left\{ \frac{\text{Tr}[\hat{\mathcal{A}}_{\nu\eta\mu} \gamma_5] k^\eta}{\mathcal{D}_{A1}} \phi_B^+(\omega) + \frac{\text{Tr}[\hat{\mathcal{A}}_{\nu\eta\mu} \gamma^\alpha \gamma_5] k^\eta}{2\mathcal{D}_{A1}} \overleftarrow{\partial}_\alpha \Phi_B^\pm(\omega) \right\} \\
&= i p_\nu q_\mu \Pi^{(A1)}(p^2, q^2) + \dots,
\end{aligned} \tag{4.9}$$

where we use short-hand notations for the Dirac structure:

$$\hat{\mathcal{A}}_{\nu\eta\mu} \equiv \gamma_\nu \gamma_5 (\omega \not{\psi} - \not{\psi} - m_s) \gamma_\rho (\omega \not{\psi} - \not{\psi} + \not{k} - m_s) \sigma_{\rho\eta} (1 + \gamma_5) (m_b \not{\psi} - \not{\psi} + m_b) \gamma_\mu (1 + \not{\psi}),$$

and for the denominator:

$$\mathcal{D}_{A1} \equiv (\omega v - p)^2 ((m_b v - q)^2 - m_b^2) k^2 (\omega v - p + k)^2,$$

where we neglect m_s^2 in the s -quark propagators. In the above, $C_F = (N_c^2 - 1)/(2N_c)$ is the standard colour factor, and $v = p_B/m_B$ is the velocity four-vector. To keep compact the second term in the above, we introduce the four-vector $\ell^\alpha \equiv \omega v^\alpha$ and define the differential operator $\overleftarrow{\partial}_\alpha \equiv \overleftarrow{\partial}/\partial\ell^\alpha$ acting on the hard-scattering kernel.

The loop momentum integration in (4.9) is from this point onward performed in $D = 4 - 2\varepsilon$ dimensions. Both ultraviolet (UV) and infrared (IR) divergences arising from the loop integrals are dimensionally regularised. Note that the $1/\varepsilon$ terms appear only in polynomial structures in p^2 , which are removed upon Borel transform in this variable. Note also that we only retain linear terms in the s -quark mass m_s , while the $\mathcal{O}(m_s^2)$ and higher-order terms are neglected, being numerically insignificant.

The expression in (4.9) has a typical factorised structure: the long-distance part represented by the B -meson distribution amplitudes $\phi_B^+(\omega)$ and $\Phi_B^\pm(\omega)$ is convoluted with the hard kernel represented by the coefficients containing traces and denominator factors. After performing the loop momentum integration, the invariant amplitude reduces to:

$$\begin{aligned}
\Pi^{(A1)}(p^2, q^2) &= -f_B \frac{m_B}{m_b} \left(\frac{\alpha_s C_F}{32\pi} \right) C_{8g} Q_b \int_0^\infty d\omega \left\{ \frac{1}{(\omega v - p)^2} \int_0^1 dx \left[(\tilde{B}_0^{(0,\phi)} \mathcal{I}_{2,0} \right. \right. \\
&+ \tilde{B}_1^{(0,\phi)} \mathcal{I}_{2,1}) \phi_B^+(\omega) + \left((\tilde{B}_0^{(1,\Phi)} + \tilde{B}_0^{(2,\Phi)}) \mathcal{I}_{2,0} + (\tilde{B}_1^{(1,\Phi)} + \tilde{B}_1^{(2,\Phi)}) \mathcal{I}_{2,1} \right. \\
&+ \left. \left. \frac{\tilde{B}_0^{(3,\Phi)}}{(\omega v - p)^2} \mathcal{I}_{2,0} + \frac{\tilde{B}_1^{(3,\Phi)}}{(\omega v - p)^2} \mathcal{I}_{2,1} + x (\tilde{B}_0^{(4,\Phi)} \mathcal{I}_{3,0} + \tilde{B}_1^{(4,\Phi)} \mathcal{I}_{3,1}) \right) \frac{\Phi_B^\pm(\omega)}{2} \right] \right\},
\end{aligned} \tag{4.10}$$

where the coefficients

$$\tilde{B}_i^{(j,\phi(\Phi))} = \tilde{B}_i^{(j,\phi(\Phi))}(p^2, q^2, m_B, m_b, m_s, x, \omega), \quad (i = 0, 1; j = 0, \dots, 4),$$

are polynomial functions of the external momenta squared, of the quark and B -meson masses, and of the Feynman parameter x . Their expressions are given in Appendix D. The loop-momentum integrals multiplied by these coefficients are defined as:

$$\mathcal{I}_{n,r} = \int \frac{d^D k}{i(2\pi)^D} \frac{(k^2)^r}{(k^2 - \Delta_{A1})^n}, \tag{4.11}$$

using the following notation:

$$\Delta_{A1} \equiv x(x-1)(\omega v - p)^2 = x(x-1)(1-\hat{\omega})(p^2 - \tilde{s}), \quad (4.12)$$

where

$$\hat{\omega} \equiv \frac{\omega}{m_B}, \quad \tilde{s} = \hat{\omega} m_B^2 - \frac{\hat{\omega}}{1-\hat{\omega}} q^2.$$

In what follows, we also use notation for the duality threshold in terms of the variable $\hat{\omega}_0$:

$$\hat{\omega}_0 = \frac{s_0 + m_B^2 - q^2 - \sqrt{(s_0 + m_B^2 - q^2)^2 + 4m_B^2(m_s^2 - s_0)}}{2m_B^2}.$$

Our main goal is to represent the result for the invariant amplitude $\Pi^{(A1)}(q^2, p^2)$ in the form of dispersion relation (3.6) in the variable p^2 at fixed $q^2 < 0$. Integrating $\mathcal{I}_{n,r}$ over loop momentum in (4.10), yields well-defined analytical structure in p^2 . More specifically, terms originating from the loop-momentum integrals contain $1/\Delta_{A1}$ or $\ln(\Delta_{A1})$, yielding, respectively, poles and logarithmic cuts at $p^2 = s > 0$, as seen from the transformed form of Δ_{A1} in (4.12). In their turn, the coefficients $\tilde{B}_i^{(j,\phi(\Phi))}$ have only polynomial dependence on p^2 , hence in these coefficients p^2 can be effectively replaced by s , anticipating Borel transform. The resulting OPE spectral density $(1/\pi)\text{Im}_s \Pi^{(A1)}(q^2, s)$ (see Appendix C for imaginary parts of different functions), is then inserted in the dispersion integral (3.6). Applying the Borel transform of the latter with respect to p^2 and subtracting the continuum contribution above the effective threshold s_0 in accordance with duality approximation, leads to the final expression for the contribution of diagram (A1) in the form ready to be inserted in LCSR (4.5):

$$\begin{aligned} I^{(A1)}(M^2, q^2) = & \frac{-1}{(4\pi)^2} \frac{1}{m_b^2} \left\{ \int_0^{\hat{\omega}_0} d\hat{\omega} e^{\frac{-s}{M^2}} \int_0^1 dx \left[\log \left(\frac{(x^2-x)(1-\hat{\omega})}{\mu^2} \right) \left(\frac{\tilde{B}_0^{(0,\phi)}}{(1-\hat{\omega})} \phi_B^+(\omega) \right. \right. \right. \\ & + \left(\frac{\tilde{B}_0^{(1,\Phi)} + \tilde{B}_0^{(2,\Phi)}}{(1-\hat{\omega})} - \frac{1}{M^2} \frac{\tilde{B}_0^{(3,\Phi)}}{(1-\hat{\omega})^2} + \frac{\tilde{B}_0^{(3,\Phi)}}{(1-\hat{\omega})^2} + 2 \frac{\tilde{B}_1^{(3,\Phi)}}{(1-\hat{\omega})} (x^2-x) \right. \\ & + \left. \left. \left. 2x \frac{\tilde{B}_1^{(4,\Phi)}}{(1-\hat{\omega})} \right) \frac{\Phi_B^\pm(\omega)}{2} \right) - x \frac{\tilde{B}_1^{(4,\Phi)}}{(1-\hat{\omega})} \frac{\Phi_B^\pm(\omega)}{2} - \frac{1}{1-x} \left(-\frac{1}{M^2} \frac{\tilde{B}_0^{(4,\Phi)}}{(1-\hat{\omega})^2} \right. \right. \\ & + \left. \left. \frac{\tilde{B}_0^{(4,\Phi)}}{(1-\hat{\omega})^2} \right) \frac{\Phi_B^\pm(\omega)}{2} + \left(\frac{-1}{M^2} \frac{\tilde{B}_0^{(3,\Phi)}}{(1-\hat{\omega})^2} + \frac{\tilde{B}_0^{(3,\Phi)}}{(1-\hat{\omega})^2} + \frac{\tilde{B}_1^{(3,\Phi)}}{(1-\hat{\omega})} (x^2-x) \right) \frac{\Phi_B^\pm(\omega)}{2} \right]_{s=\tilde{s}} \\ & + \int_{m_s^2}^{s_0} ds \int d\hat{\omega} \int_0^1 dx \left[\frac{1}{(1-\hat{\omega})} \frac{d}{ds} \left((\tilde{B}_0^{(0,\phi)} \phi_B^+(\omega) + (\tilde{B}_0^{(1,\Phi)} + \tilde{B}_0^{(2,\Phi)} \right. \right. \\ & + \left. \left. 2\tilde{B}_1^{(3,\Phi)} (x^2-x) + 2\tilde{B}_1^{(4,\Phi)} x) \frac{\Phi_B^\pm(\omega)}{2} \right) e^{\frac{-s}{M^2}} \right) \Theta(s-\tilde{s}) \log |s-\tilde{s}| \\ & - 2(x^2-x) \left(\tilde{B}_1^{(0,\Phi)} \phi_B^+(\omega) + (\tilde{B}_1^{(1,\Phi)} + \tilde{B}_1^{(2,\Phi)}) \frac{\Phi_B^\pm(\omega)}{2} \right) e^{\frac{-s}{M^2}} \Theta(s-\tilde{s}) \\ & \left. - \frac{1}{(1-\hat{\omega})^2} \frac{d^2}{ds^2} (\tilde{B}_0^{(3,\Phi)} e^{\frac{-s}{M^2}}) \log |s-\tilde{s}| \Theta(s-\tilde{s}) \frac{\Phi_B^\pm(\omega)}{2} \right] \left. \right\}, \quad (4.13) \end{aligned}$$

where $\tilde{B}'_i^{(j,\Phi)}$ is the derivative of $\tilde{B}_i^{(j,\Phi)}$ with respect to the variable s . The remaining form-factor-like contributions from diagrams (A2), (A3) and (B1), (B2), (B3) yield analogous invariant amplitudes $I^{(A2)}$, $I^{(A3)}$ and $I^{(B1)}$, $I^{(B2)}$, $I^{(B3)}$ respectively, as provided in Appendix D. Their coefficient functions denoted, respectively, as $\tilde{C}_i^{(j,\phi(\Phi))}$, $\tilde{A}_i^{(j,\phi(\Phi))}$ and $\bar{A}_i^{(j,\phi(\Phi))}$, $\bar{C}_i^{(j,\phi(\Phi))}$, $\bar{B}_i^{(j,\phi(\Phi))}$ are given in the ancillary file.

As already explained in the previous section at a qualitative level, the remaining diagrams (A4) and (B4) do not develop an imaginary part in p^2 within the duality interval, characteristic for the kaon channel and therefore do not contribute to the LCSR (4.5). To substantiate this statement with a direct computation, we consider e.g. diagram (A4). After loop-momentum integration, the only propagator in this diagram which retains a dependence on the variable p^2 , has the denominator equal to

$$(\omega v - q)^2 = \hat{\omega} \left(p^2 - ((1 - \hat{\omega})m_B^2 - \frac{1 - \hat{\omega}}{\hat{\omega}}q^2) \right).$$

At $q^2 < 0$, this expression vanishes, yielding a pole at $p^2 \gtrsim \mathcal{O}(m_B^2 + |q^2|)$ in the diagram expression. That pole is indeed well above the duality interval for the kaon channel. The same reasoning applies to diagram (B4) and also to diagram (D3) with soft gluon.

An important and nontrivial property of the form-factor-like diagrams is that their expressions are complex valued at $q^2 < 0$. The imaginary part is revealed for the diagrams (A1), (A2), (A3), as well as (B2). The emergence of imaginary part at spacelike q^2 is a known feature of $b \rightarrow s\gamma^*$ diagrams at NLO calculated for the inclusive $b \rightarrow s\ell^+\ell^-$ process [17] (see a detailed discussion in [7]). An interesting question which is beyond our scope is the interpretation of these discontinuities in terms of intermediate on-shell hadronic states. As a result, the dispersion relation (3.6) should be understood as a linear combination of two separate dispersion relations, splitting the integrand $\text{Im}_{p^2}\Pi^{(OPE)}(s, q^2)$ into a real and imaginary part.

4.3 Hard-scattering diagrams

We now turn to the hard-scattering contributions represented by diagrams (C1)–(C4). These diagrams all contain hard gluon emitted from the chromomagnetic operator and absorbed by the spectator quark. They enter the sum rule at the same order in α_s as the form-factor-like diagrams discussed in Sec. 4.2.

As an explicit example, we consider diagram (C1), where the photon is emitted from the b -quark line. The corresponding contribution to the correlation function (3.1) reads:

$$\begin{aligned} \Pi_{\nu\mu}^{(C1)}(q, p) &= -if_B m_B \left(\frac{\alpha_s C_F}{32\pi} \right) m_b C_{8g} Q_b \int_0^\infty d\omega \int \frac{d^4k}{(2\pi)^4} \\ &\times \left\{ \frac{\text{Tr}[\hat{\mathcal{C}}_{\nu\eta\mu} \gamma_5] k^\eta}{\mathcal{D}_{C1}} \phi_B^+(\omega) + \frac{\text{Tr}[\hat{\mathcal{C}}_{\nu\eta\mu} \gamma^\alpha \gamma_5] k^\eta}{2\mathcal{D}_{C1}} \partial_\alpha \Phi_B^\pm(\omega) \right\}, \\ &= ip_\nu q_\mu \Pi^{(C1)}(p^2, q^2) + \dots, \end{aligned} \quad (4.14)$$

where the Dirac structure $\hat{\mathcal{C}}$ is given by:

$$\hat{\mathcal{C}}_{\nu\eta\mu} \equiv \gamma_\rho (\not{k} + \omega \not{\psi}) \gamma_\nu \gamma_5 (\not{k} + \omega \not{\psi} - \not{p} - m_s) \sigma_{\rho\eta} (1 + \gamma_5) (m_b \not{\psi} - \not{q} + m_b) \gamma_\mu (1 + \not{\psi}),$$

and the short-hand notation for the denominator is introduced:

$$\mathcal{D}_{C1} \equiv ((m_b v - q)^2 - m_b^2) k^2 (k + \omega v)^2 (k + \omega v - p)^2.$$

After performing the loop-momentum integration, transforming the invariant amplitude $\Pi^{(C1)}(p^2, q^2)$ to a form of dispersion relation in p^2 , followed by Borel transform and continuum subtraction, the expression we obtain for the contribution of the diagram (C1) to LCSR turns out rather cumbersome. We found the way to simplify that, applying a transformation of Feynman parameters, $x_1 = X y_1$ and $x_2 = X(1 - y_1)$, such that $x_1 + x_2 = X$ and $0 \leq X, y_1 \leq 1$. The corresponding Jacobian is $|J| = X$, and we define

$$\begin{aligned}\mathcal{W}_{C1} &= -\bar{y}_1 (\bar{\omega} \bar{X} + X y_1), \\ \mathcal{X}_{C1} &= -\hat{\omega} \bar{X} ((q^2 - m_B^2) \bar{y}_1 - m_B^2 \hat{\omega}),\end{aligned}\tag{4.15}$$

where the barred variables are introduced as, e.g., $\bar{X} = 1 - X$.

With these definitions, we obtain:

$$\begin{aligned}I^{(C1)}(M^2, q^2) &= - \int_{m_s^2}^{s_0} ds e^{-s/M^2} \int_0^\infty d\hat{\omega} \int_0^1 dX dy_1 \frac{1}{m_b^2} \left\{ \left[D_0^{(0,\phi)} \frac{\delta(\mathcal{W}_{C1}s - \mathcal{X}_{C1})}{\mathcal{W}_{C1}} \right. \right. \\ &\quad \left. \left. - 2X D_1^{(0,\phi)} \Theta(\mathcal{X}_{C1} - \mathcal{W}_{C1}s) \right] \phi_B^+(\omega) + \left[\left(D_0^{(1,\Phi)} + D_0^{(2,\Phi)} \right. \right. \right. \\ &\quad \left. \left. + \frac{(y_1 D_0^{(3,\Phi)} + (1 - y_1) D_0^{(4,\Phi)})}{M^2} + (y_1 D_0'^{(3,\Phi)} + (1 - y_1) D_0'^{(4,\Phi)}) \right. \right. \\ &\quad \left. \left. + 2X (y_1 D_1^{(3,\Phi)} + (1 - y_1) D_1^{(4,\Phi)}) \right) \frac{\delta(\mathcal{W}_{C1}s - \mathcal{X}_{C1})}{\mathcal{W}_{C1}} \right. \\ &\quad \left. \left. - 2X (D_1^{(1,\Phi)} + D_1^{(2,\Phi)}) \Theta(\mathcal{X}_{C1} - \mathcal{W}_{C1}s) \right] \frac{\Phi_B^\pm(\omega)}{2} \right\},\end{aligned}\tag{4.16}$$

where the δ -function fixes the domain of the integration region, while the Θ -function implements the continuum subtraction. The treatment of the δ -function is standard and reads:

$$\int_0^1 dX f(X) \delta(\mathcal{W}_{C1}s - \mathcal{X}_{C1}) = \frac{f(X_0)}{\left(\frac{\partial}{\partial X} (\mathcal{W}_{C1}s - \mathcal{X}_{C1}) \right) \Big|_{X=X_0}} \Theta(0 < X_0 < 1).\tag{4.17}$$

The remaining hard-scattering contributions to LCSR: $I^{(C2)}$, $I^{(C3)}$, and $I^{(C4)}$, are obtained analogously. Their explicit analytical forms are provided in Appendix D. The corresponding coefficient functions denoted as $B_i^{(j,\phi(\Phi))}$, $A_i^{(j,\phi(\Phi))}$, and $C_i^{(j,\phi(\Phi))}$ for diagrams (C2), (C3), and (C4), respectively are presented in the ancillary file.

We also note that, in contrast with the form-factor-like contributions, none of the hard-scattering diagrams (C1)–(C4) develops an imaginary part in the spacelike region $q^2 < 0$.

4.4 Soft-gluon diagrams

In addition to the hard-gluon contributions discussed above, the correlation function (3.1) involves diagrams, in which a low-virtuality gluon belonging to the B -meson long-distance structure is exchanged with the chromomagnetic operator O_{8g} . These are diagrams (D1)–(D3) described in terms of B -meson three-particle DAs, convoluted with a short-distance kernel, which is represented by two off-shell quark propagators. The relevant definitions and the explicit parameterisations of the three-particle DAs are collected in Appendix B.

We only have to evaluate diagrams ($D1$) and ($D2$), where the virtual photon is emitted, respectively, from the b -quark and s -quark lines. As discussed in Sec. 4.2, diagram ($D3$) with a photon emission from the spectator quark does not contribute to the sum rule, since the corresponding pole in p^2 lies far away from the duality interval of the kaon channel.

As an explicit example, we discuss a soft-gluon contribution from diagram ($D1$), corresponding to a virtual photon emission from the b -quark. This computation is naturally simpler than in the case of hard-gluon diagrams, due to absence of the loop. Contracting the b and s -quark fields into propagators, we decompose the vacuum-to- B matrix element of the remaining b , \bar{s} and gluon fields into a combination of B -meson three-particle DAs. After performing the coordinate integration, the resulting invariant amplitude takes the form:

$$\begin{aligned} \Pi^{(D1)}(p^2, q^2) = & \sum_{n=1,2} \frac{f_B m_b}{8\pi^2} C_{8g} \int_0^\infty d\omega \int_0^\infty d\xi \frac{1}{[(\omega v - p)^2]^n} \left[F_n^{(\Psi_{AV})}(q^2, \omega) (\Psi_A(\omega, \xi) - \Psi_V(\omega, \xi)) \right. \\ & + F_n^{(\Psi_V)}(q^2, \omega) \Psi_V(\omega, \xi) + F_n^{(X_A)}(q^2, \omega) \bar{X}_A(\omega, \xi) + F_n^{(W_{YA})}(q^2, \omega) (\bar{W}(\omega, \xi) \\ & \left. + \bar{Y}_A(\omega, \xi)) + F_n^{(\tilde{X}_A)}(q^2, \omega) \bar{\tilde{X}}_A(\omega, \xi) + F_n^{(\tilde{Y}_A)}(q^2, \omega) \bar{\tilde{Y}}_A(\omega, \xi) \right]. \end{aligned} \quad (4.18)$$

The coefficient functions $F_n^{(X)}$, where X stands for a three-particle DA, are given in Appendix E. Our result supersedes the earlier calculation of the same diagrams in [7], by including a complete set of three-particle DAs. We also spotted a difference in one of the coefficients, (see Appendix E for details) which however has a negligible impact on the numerical results.

A transition from the above expression for the invariant amplitude to a final integral over spectral density $I^{(D1)}(M^2, q^2)$, obtained after casting in a dispersion form, Borel transform and duality subtraction is reduced to the following replacements:

$$\begin{aligned} \int_0^\infty d\omega \frac{f(q^2, \omega)}{(\omega v - p)^2} & \rightarrow - \int_0^{\hat{\omega}_0} \frac{d\hat{\omega}}{(1 - \hat{\omega})} e^{-\bar{s}/M^2} f(q^2, \omega), \\ \int_0^\infty d\omega \frac{f(q^2, \omega)}{((\omega v - p)^2)^2} & \rightarrow \int_0^{\hat{\omega}_0} \frac{d\hat{\omega}}{(1 - \hat{\omega})^2} e^{-\bar{s}/M^2} \frac{f(q^2, \omega)}{M^2} + \frac{e^{-\bar{s}(\hat{\omega}_0)/M^2} f(q^2, \hat{\omega}_0)}{m_B (1 - \hat{\omega}_0)^2 \left(1 - \frac{q^2}{m_B^2 (1 - \hat{\omega}_0)^2}\right)}. \end{aligned} \quad (4.19)$$

The remaining soft-gluon diagram ($D2$) is computed in an analogous way. Its final expression is provided in Appendix D and the associated coefficient functions denoted as $\tilde{F}_n^{(X)}$ are collected in the ancillary file.

4.5 Power counting

Since we have at hand all contributions to the LCSR (3.8) calculated within one and the same approach and input, it is instructive to investigate the hierarchy of these contributions with respect to the powers of inherent large scales. In general, here we deal with the following parametric hierarchy of scales:

$$\{m_b, m_B\} \gg \{\sqrt{|q^2|}, \mu, M\} \gg \{\Lambda_{QCD}, \sqrt{s_0}, \bar{\Lambda}\} \equiv \Lambda, \quad (4.20)$$

where μ (M) is the renormalisation (Borel) scale and on r.h.s. we introduce a generic hadronic scale $\Lambda \lesssim 1$ GeV which spans from Λ_{QCD} to $\bar{\Lambda} = m_B - m_b$.

Within the LCSR framework, the non-perturbative input is provided by the B -meson DAs, depending on the momentum variable $\omega \sim \mathcal{O}(\Lambda)$. The latter condition is justified, since the realistic models of B -meson DAs are suppressed at large ω . Moreover, the characteristic soft scale of these distributions is governed by the inverse moment λ_B of the leading-twist DA $\phi_B^+(\omega)$, defined in (B.6), and this parameter is also of $\mathcal{O}(\Lambda)$.

Taking into account the scale hierarchy, discussed above, we analysed the relative role of separate diagrams in LCSR. The contribution of each diagram to the invariant amplitude of the correlation function can be represented as a convolution of the perturbatively calculable hard kernel with the B -meson DA. Schematically, up to the common prefactor $(C_F/2)(f_B m_B/4)m_b$, these amplitudes take the form

$$\Pi^{(X)} \sim \int_0^\infty d\omega \phi_B^+(\omega) K^{(X)}(\omega, q^2) + (\Phi_B^\pm\text{-term}), \quad (4.21)$$

where $(X) = (A1), \dots$ labels the individual diagrams. For $(D1)$ and $(D2)$, the two-particle DAs are replaced with three-particle DAs. Determined by the dependence of the kernels $K^{(X)}$ on the variables ω and q^2 , the amplitudes $\Pi^{(X)}$ for each category of diagrams reveal distinctively different parametric values:

- for the form-factor-like diagrams (A, B) , we obtain $K(\omega) \propto 1/\omega$, yielding

$$\Pi^{(A+B)} \sim \left(\frac{\alpha_s}{4\pi}\right) \frac{1}{\lambda_B} \left[1 + \mathcal{O}\left(\frac{\Lambda}{m_B}\right)\right], \quad (4.22)$$

- for the hard-scattering diagrams (C) , $K(\omega) \propto (1/\omega) \times \mathcal{O}(\Lambda/m_B)$, yielding

$$\Pi^{(C)} \sim \left(\frac{\alpha_s}{4\pi}\right) \frac{1}{\lambda_B} \times \mathcal{O}\left(\frac{\Lambda}{m_B}\right), \quad (4.23)$$

- the soft-gluon diagrams (D) involve three-particle B -meson DAs with normalisation $\lambda_{E,H}^2 \sim \mathcal{O}(\Lambda^2)$, leading to

$$\Pi^{(D)} \sim \frac{1}{\lambda_B} \times \mathcal{O}\left(\frac{\lambda_{E,H}^2}{m_B^2}\right). \quad (4.24)$$

Note that the power hierarchy of diagrams obtained above does not change after Borel transform and duality subtraction. We come to a conclusion that in the O_{8g} contribution to the nonlocal form factor, the diagrams with form-factor-like topologies are parametrically leading while both hard-scattering and soft-gluon contributions are suppressed by at least one power of $\mathcal{O}(\Lambda/m_B)$. Moreover, albeit the soft-gluon contribution is suppressed by additional power of Λ/m_B with respect to the hard-scattering contribution, this extra power suppression can be compensated by $\alpha_s/4\pi$ which is numerically of the same order.

5 Numerical Results

We begin with the numerical evaluation of the LCSR in (3.8) in the region $q^2 < 0$. The input values of quark and meson masses, e.m. and strong couplings, together with the decay constants of B -meson and kaon are collected in Table 1. Since our calculation is performed at spacelike momentum transfer, we employ the $\overline{\text{MS}}$ scheme. The expressions of the B -meson DAs used in our analysis are given in Appendix B. They are determined by two independent parameters for which we adopt QCD sum rule estimates. In particular, for the inverse

Parameter	Value	Ref.
m_{K^0}	497.611 ± 0.013 MeV	[24]
m_{B^0}	5279.63 ± 0.20 MeV	[24]
m_b	4.183 ± 0.004 GeV	[24]
m_c	1.2730 ± 0.0046 GeV	[24]
α_{em}	1/128	[24]
$\alpha_s(m_Z)$	0.1180 ± 0.0009	[24]
f_B	190.0 ± 1.3 MeV	[25]
f_K	155.7 ± 0.3 MeV	[25]
λ_B	460 ± 110 MeV	[18]
$R(\equiv \lambda_E^2/\lambda_H^2)$	$0.3^{+0.17}_{-0.12}$	see text
M^2	1.0 ± 0.5 GeV ²	see text
s_0	1.05 ± 0.05 GeV ²	see text

Table 1: Input parameters used in the numerical evaluation of the LCSR (3.8).

moment of the twist-2 DA, λ_B , we take the result of [18] (a close interval was obtained later in [19]). For the ratio $R = \lambda_E^2/\lambda_H^2$ of the parameters characterising quark-antiquark-gluon DAs, we use the average of two independent sum rule analyses [20] and [21]³.

Furthermore, for the two specific parameters of LCSR (3.8), the Borel mass M and effective threshold s_0 for the channel of the kaon interpolation current, it is natural to adopt the values in the same ballpark as for the analogous LCSRs with B -meson DAs for the $B \rightarrow K$ local form factors. In the original analysis [12] of the latter sum rule, the interval $M^2 = 1.0 \pm 0.5$ GeV² was taken, together with the value $s_0 = 1.05$ GeV². These values were taken from the earlier analysis [22] of two-point sum rules for the kaon decay constant in the same channel of the kaon interpolating current (3.2). In the later update [23] of the LCSR for the $B \rightarrow K$ form factors, the same interval for the Borel mass was taken and for s_0 a small uncertainty was included which we double. To stay on a conservative side, we also assume that the Borel mass and the effective threshold are uncorrelated.

To adopt an optimal scale for strong coupling and quark masses, we note that the typical virtuality of the hard kernel is in the ballpark of $m_b \Lambda_{\text{QCD}}$. Accordingly, we evaluate the scale-dependent amplitude $\mathcal{H}^{BK,Os}(q^2)$ given by the LCSR (3.8) at $\mu = 2$ GeV. Varying the scale around this value, we find that noticeable scale dependence is revealed mainly, through the form-factor-like contributions of diagrams (A) and (B), while the hard-scattering and soft-gluon terms are almost insensitive to μ . We also neglect possible renormalisation effects of the DAs, in particular the scale-dependence of the inverse moment λ_B , having in mind a large uncertainty of this quantity.

According to our definition (2.3), the nonlocal form factor $\mathcal{H}^{(BK,Os)}(q^2)$ determined from LCSR (3.8) contains the Wilson coefficient C_{8g} as a factor. We consider the scale of this coefficient, as well as of the coefficients $C_{1,2}$ entering the ratio (2.4), to be independent of the scale we use to calculate the nonlocal form factor from LCSR. In our numerical analysis

³This average is kindly provided by Aritra Biswas.

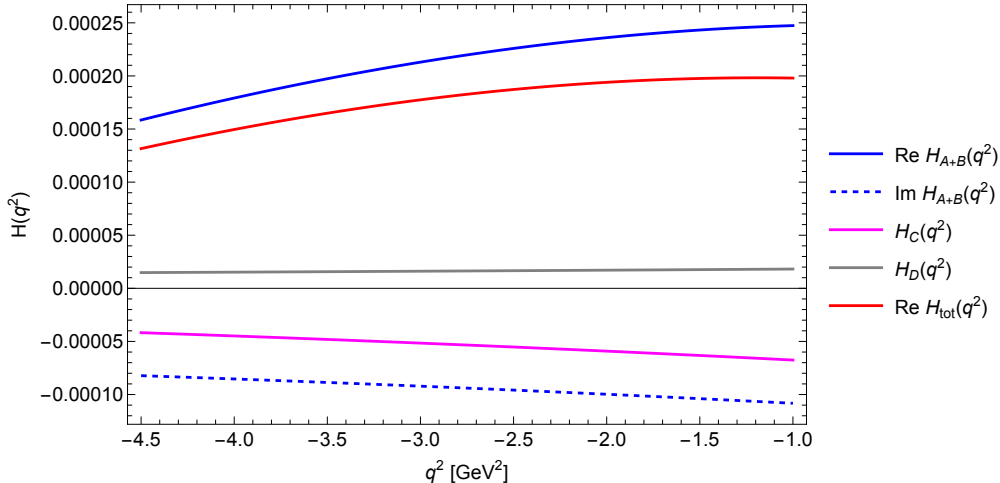


Figure 2: Individual contributions to the rescaled non-local form factor for the operator O_{8g} , defined according to (5.1), in the spacelike region $q^2 < 0$. The blue and dashed-blue lines represent the real and imaginary parts of the form-factor-like contribution H_{A+B} , respectively. The magenta and gray curves correspond to the hard-scattering and soft-gluon contributions, H_C and H_D . The total real part, $\text{Re } H_{\text{tot}}(q^2)$, obtained from their coherent sum, is shown in red.

we use $C_1(m_b) = 1.010$, $C_2(m_b) = -0.290$, $C_{8g}(m_b) = -0.171$ [26].

For numerical illustration, it is more convenient to isolate the “genuine” hadronic amplitude determined from LCSR from this short-distance factor, introducing

$$H(q^2) \equiv \frac{\mathcal{H}^{(BK, O_8)}(q^2)}{C_{8g}}. \quad (5.1)$$

Figure 2 displays the real and imaginary parts of different contributions to this quantity, according to the classification defined in Secs. 4.2–4.4. For consistency, in all diagrams, the B -meson DAs up to twist-3 are included.

The form-factor-like diagrams, labeled (A, B) , yield the dominant part of the nonlocal form factor, while the hard-scattering (C) and soft-gluon (D) diagrams are suppressed by approximately one order of magnitude, in agreement with the power-counting analysis presented in Sec. 4.5. The imaginary part of $(A + B)$ originates entirely from the logarithmic branch cuts of the hard kernel and remains small throughout the spacelike region. Notice that the nonlocal contributions from O_{8g} exhibit only a mild q^2 dependence across the considered spacelike region.

Furthermore, Figure 3 displays the ratio (2.4) in the spacelike q^2 region. Here, we take the prediction of LCSR for $B \rightarrow K$ form factor at negative q^2 from [23], where the full higher-twist contributions for three-particle DAs are included. This choice is consistent with the approximation adopted in our calculation, and in accordance with using the same Borel interval and threshold in the kaon channel. The real part of the ratio is negative and dominated by the form-factor-like term R_{A+B} (blue), while the hard-scattering and soft-gluon pieces R_C (magenta) and R_D (gray) are suppressed. The imaginary part (dashed blue), arising from the logarithmic branch cuts, remains small. The overall magnitude of $|R_{\text{tot}}(q^2)| \lesssim 6 \times 10^{-3}$ indicates that the O_{8g} contribution is strongly suppressed compared to the $O_{1,2}^c$ term. Importantly, in this suppression the ratio of Wilson coefficients acts in the opposite direction, since the ratio (2.4) contains a factor $C_{8g}/(C_1/3 + C_2) > 1$.

For the soft-gluon contributions, we also studied the effect of additional three-particle

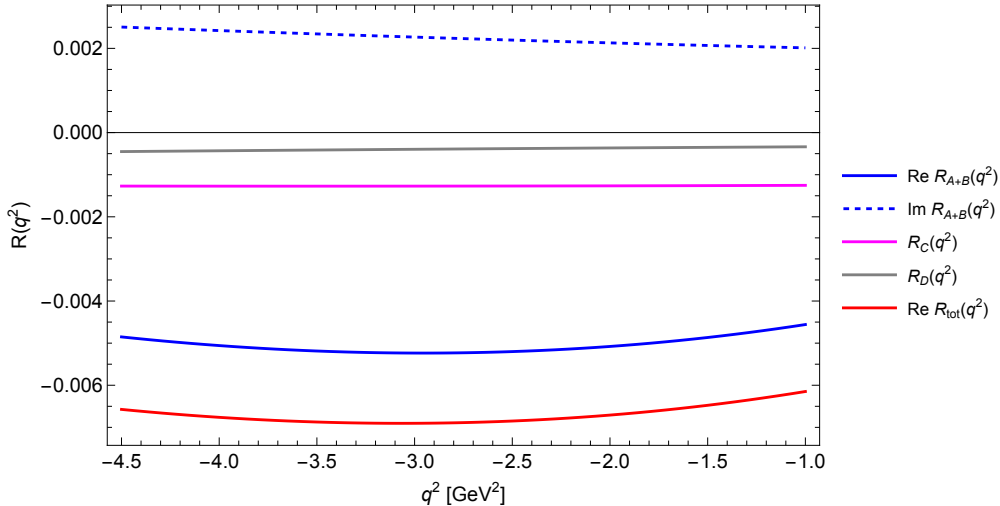


Figure 3: The blue (solid and dashed) lines show the real and imaginary parts of the factorisable term, while the magenta and gray curves represent the nonfactorisable hard- and soft-gluon pieces. The total ratio $\text{Re } R_{\text{tot}}(q^2)$ is shown in red.

Nonlocal form factor $H^{(BK,Os)}$ and its components at $q^2 = -4.0 \text{ GeV}^2$ (in units of 10^{-4})				
γ^*	form-factor-like (A)	form-factor-like (B)	hard-scattering (C)	soft-gluon (D)
(1)	$0.046 + i 0.014$	0.436	0.205	0.297
(2)	$0.446 - i 0.623$	$0.482 - i 0.272$	-0.180	-0.150
(3)	$0.007 - i 0.04$	0.562	-0.409	0
(4)	0	0	-0.099	-
subtotal	$1.979(0.146) - i 0.885(0.155)$		-0.482(0.251)	0.151(0.024)
total	$1.648(0.291) - i 0.885(0.155)$			

Table 2: The entries (1)–(4) in the first column correspond to the different photon emission topologies illustrated in Fig. 1. The columns list the separate form-factor-like (A, B), hard-scattering (C), and soft-gluon (D) components.

B -meson DAs not included in [7] and found that the numerical impact of this modification is inessential.

As another numerical illustration, in Table 2 we present our results for the nonlocal form factor generated by the O_{8g} operator at a momentum transfer squared $q^2 = -4.0 \text{ GeV}^2$. As previously found, the spectator-emission configurations (A4) and (B4) do not develop spectral density dual to the kaon pole in the dispersion relation and therefore vanish, as indicated in Table 2.

To obtain the uncertainties quoted in this table, we used a Monte Carlo approach, sampling the input parameters M^2 , s_0 , λ_B , R , and f_B as independent variables. For λ_B , R , and f_B we employ Gaussian distributions with central values and standard deviations taken from Table 1. For the Borel parameter M^2 and the effective threshold s_0 , truncated Gaussian distributions are used to avoid going beyond the validity of the permitted Borel window. The error for each of the twelve subdiagrams is computed individually; the resulting errors are then added in quadrature to obtain the uncertainty for each diagram class, and finally for the total result.

It is instructive to compare our new results for the hard-gluon contributions with the

existing results in the literature obtained in the framework of QCdf. However, one has to keep in mind that such a comparison is rather qualitative, because our diagrammatic classification in the LCSR framework does not have a one-to-one correspondence with QCdf diagrams.

In particular, we compare the form-factor-like contributions (the sum of diagrams (A) and (B)) obtained here, with the similar contribution to QCdf at $q^2 < 0$, using the hard-gluon $b \rightarrow s\gamma^*$ kernel calculated at NLO in [17] and cast into a form of the coefficient function $F_8^{7,9}$. This kernel is then factorised with the local $B \rightarrow K$ form factor (see [7], where this contribution was estimated at $q^2 < 0$). Using the analytical expression for the function $F_8^{7,9}$ and the local $B \rightarrow K$ form factor from [23], we obtain, at the central values of the input:

$$H_{(A+B)}^{(BK,O_8)} \Big|_{QCdf} = (1.39 - i0.84) \times 10^{-4},$$

in the same ballpark as our numerical estimate from LCSR presented in Table 2.

For the hard-scattering contributions, our LCSR includes all four diagrams, (C1)–(C4). In the original QCdf analysis [5], only the diagram analogous to (C4) is taken into account, and the remaining diagrams are not included, being power-suppressed, according to the power-counting in QCdf. In contrast, in LCSR, the contributions of all four hard-scattering diagrams are of the same order. On the other hand, we find a strong numerical cancellation between the diagrams (C1) and (C2). This effect is caused by opposite signs of these diagrams, where in (C₁) ((C₂)) the virtual photon is emitted from the incoming b -quark (outgoing s -quark). After this cancellation, the resulting hard-scattering contribution presented in Table 2 is smaller than the form-factor-like one. Our result has the same sign and a compatible magnitude with the estimate

$$H_{(C)}^{(BK,O_8)} \Big|_{QCdf} = -0.78 \times 10^{-4},$$

that we obtain using the formula for the hard-scattering diagram in QCdf derived in [5].

For the soft-gluon contributions given by diagrams (D1)–(D2), it is important to compare our result presented in Table 2 with the previous calculation done within the same LCSR method in [7]. The difference between these two calculations are: (i) a slight difference in the formula for the coefficient $F_1^{(XA)}$ in the LCSR, and (ii) a more complete set of B -meson three-particle DAs employed here and taken from [15]. Using the expression presented in [7] we recalculated the soft-gluon contribution and found:

$$H_{(D)}^{(BK,O_8)} \Big|_{LCSR[7]} = 0.159 \times 10^{-4},$$

very close to our current estimate. This comparison indicates that both differences mentioned above are irrelevant for the numerical results. In fact, the B -meson three-particle DAs of higher than three twists, have an insignificant impact on the numerical result for the soft-gluon contribution.

Note that the numerical analysis carried out here does not take into account renormalisation effects related to the O_{8g} operator, such as the scale-dependence or mixing with four-quark operators. These effects will become relevant when contributions of other effective operators to the nonlocal form factor will be computed in a future work.

6 Conclusion and outlook

In this paper, for the first time, we demonstrated that it is possible to compute the nonlocal form factor in $B \rightarrow K\ell^+\ell^-$ at spacelike momentum transfer $q^2 < 0$, applying the method

of QCD LCSRs with B -meson DAs. Specifically, we obtained the contribution of the chromomagnetic penguin operator O_{8g} , a task that is technically less involved, as compared to the case of current-current operators, which demands computation of two-loop diagrams. Our main results are the contributions to the nonlocal form factor generated by hard-gluon exchanges between quarks in this hadronic matrix element. We also recalculated and slightly updated the previously known soft-gluon contributions. Importantly, the same LCSR approach is applicable to the local $B \rightarrow K$ form factors equally important for $B \rightarrow K\ell^+\ell^-$ decays.

We identify three different categories of diagrams contributing to LCSR, two of them with hard-gluon exchanges (the form-factor-like and hard-scattering diagrams) and the third category involving the soft-gluon effects. We computed and presented analytical expressions for the spectral density of all diagrams entering the LCSR. Our results confirm that the nonlocal form factor is a complex-valued quantity already at $q^2 < 0$, a property that can be interpreted as the presence of intermediate on-shell light-hadron states. We also established the power-counting scheme of different contributions, revealing the dominance of form-factor-like contributions.

Our numerical analysis shows that, compared to leading-order charm-loop contribution, the nonlocal effect in $B \rightarrow K\ell^+\ell^-$ due to the chromomagnetic penguin operator is at sub-percentage level in the spacelike region. Furthermore, comparison with the previous calculations within QCdf framework indicates a reasonable agreement.

Our future task planned for the next work in this direction is a LCSR calculation of the contributions generated by the leading $O_{1,2}^c$ operators and similar four-quark operators. We will extensively use the computational routine developed in this paper. While principal elements of the method are already worked out here, there will be additional difficulties of both technical and conceptual origin. First of all, one will deal with two-loop diagrams, including the primary charm-loop. Secondly, concerning soft-gluon effects, one will encounter a problem of a proper light-cone expansion of the correlation function, having in mind that there are three different points of quark-antiquark-gluon emission. This problem was recently discussed in detail in [27] in a context of a LCSR calculation of the $B \rightarrow D\pi$ nonleptonic decays.

We believe that the results of this work bring us one step closer to resolving the problem of nonlocal effects in the $b \rightarrow s$ FCNC transitions, providing an established QCD-based approach of LCSRs to analyse in detail this very intricate hadronic phenomenon.

Acknowledgements

We thank Alexandre Carvunis for discussions and involvement in the early stage of this project. D.M. is grateful to Thorsten Feldmann for useful comments.

The research of A.K. was supported by the German Research Foundation (DFG) under grant 396021762 - TRR 257 “Particle Physics Phenomenology after the Higgs Discovery”. A.K. and T.H. also acknowledge the hospitality during his visit to the Institut de Physique des 2 Infinis de Lyon, when this work was initiated. T.H. is supported by the Cluster of Excellence “Precision Physics, Fundamental Interactions, and Structure of Matter” (PRISMA+ EXC 2118/1) funded by the German Research Foundation (DFG) within the German Excellence Strategy (Project ID 390831469). T.H. also thanks the CERN theory group for its hospitality during his regular visits to CERN where part of the work was done. This research is funded in part by the National Research Agency (ANR) under project no. ANR-21-CE31-0002-01.

A Notations and conventions

We consider the $|\Delta B| = 1$ effective Hamiltonian [28–31]:

$$\mathcal{H}_{\text{eff}} = -\frac{4G_F}{\sqrt{2}} V_{tb} V_{ts}^* \sum_{i=1}^{10} C_i(\mu) O_i(\mu) + \text{h.c.}, \quad (\text{A.1})$$

with the operators:

$$\begin{aligned} O_1^c &= (\bar{s}_L \gamma_\mu c_L) (\bar{c}_L \gamma^\mu b_L), \\ O_2^c &= (\bar{s}_L^j \gamma_\mu c_L^i) (\bar{c}_L^i \gamma^\mu b_L^j), \end{aligned} \quad (\text{A.2})$$

where $q_{L(R)} = \frac{1-(+)\gamma_5}{2} q$ and $P_{L(R)} = \frac{1-(+)\gamma_5}{2}$. The chromomagnetic operator O_{8g} , which plays the main role in this paper is already presented in (2.1). All other effective operators entering (A.1) are not relevant here.

The sign convention adopted in this paper corresponds to the covariant derivative acting on quark field: $iD_\mu = i\partial_\mu + eQ_q A_\mu + g_s T^a A_\mu^a$, where Q_q is the quark charge. We also use $\sigma_{\mu\nu} = i/2[\gamma^\mu, \gamma^\nu]$ and the convention for the Levi-Civita tensor such that $\text{Tr}\{\gamma^\mu \gamma^\nu \gamma^\rho \gamma^\lambda \gamma^5\} = 4i\epsilon^{\mu\nu\rho\lambda}$, $\epsilon^{0123} = -1$.

B B -meson distribution amplitudes

In HQET, the nonperturbative structure of the B -meson is encoded in a set of light-cone DAs, which are defined through matrix elements of nonlocal quark-gluon operators. We collect here the conventions and expressions used in our calculations, following [15, 32].

The two-particle (quark-antiquark) LCDAs are defined through

$$\begin{aligned} \langle 0 | \bar{q}_2^\alpha(x) h_v^\beta(0) | \bar{B}_{q_2}(v) \rangle &= -\frac{i f_B m_B}{4} \int_0^\infty d\omega e^{-i\omega v \cdot x} \left\{ (1 + \not{v}) \left[\phi_+(\omega) - g_+(\omega) \not{\partial}_\sigma \not{\partial}^\sigma \right. \right. \\ &\quad \left. \left. + \left(\frac{\Phi_\pm(\omega)}{2} - \frac{\bar{g}(\omega)}{2} \not{\partial}_\sigma \not{\partial}^\sigma \right) \gamma^\mu \not{\partial}_\mu \right] \gamma_5 \right\}^{\beta\alpha}, \end{aligned} \quad (\text{B.1})$$

where h_v is the heavy-quark field in HQET, and ω represents the light-cone projection of the spectator quark momentum.

The corresponding three-particle (quark-antiquark-gluon) LCDAs are defined through

$$\begin{aligned} \langle 0 | \bar{q}_\alpha(x) G_{\mu\nu}(ux) h_{v\beta(0)} | \bar{B}(v) \rangle &= \frac{f_B m_B}{4} \int_0^\infty d\omega \int_0^\infty d\xi e^{-i(\omega+u\xi)v \cdot x} \\ &\quad \left\{ (1 + \not{v}) \left[(v_\mu \gamma_\nu - v_\nu \gamma_\mu) (\psi_A - \psi_V) - i \sigma_{\mu\nu} \psi_V \right. \right. \\ &\quad \left. \left. + (\partial_\mu v_\nu - \partial_\nu v_\mu) \bar{X}_A - (\partial_\mu \gamma_\nu - \partial_\nu \gamma_\mu) [\bar{W} + \bar{Y}_A] \right. \right. \\ &\quad \left. \left. + i \epsilon_{\mu\nu\alpha\beta} \partial^\alpha v^\beta \gamma_5 \bar{X}_A - i \epsilon_{\mu\nu\alpha\beta} \partial^\alpha \gamma^\beta \gamma_5 \bar{Y}_A - u (\partial_\mu v_\nu \right. \right. \\ &\quad \left. \left. - \partial_\nu v_\mu) \not{\partial} \bar{W} + u (\partial_\mu \gamma_\nu - \partial_\nu \gamma_\mu) \not{\partial} \bar{Z} \right] \gamma_5 \right\}_{\beta\alpha}(\omega, \xi), \end{aligned} \quad (\text{B.2})$$

where $G_{\mu\nu}$ denotes the gluon field-strength tensor. The shorthand notations for the integrated DAs are

$$\bar{\psi}_{3\text{p}}(\omega, \xi) \equiv \int_0^\omega d\tau \psi_{3\text{p}}(\tau, \xi), \quad \bar{\bar{\psi}}_{3\text{p}}(\omega, \xi) \equiv \int_0^\omega d\tau \int_0^\xi d\delta \psi_{3\text{p}}(\tau, \delta). \quad (\text{B.3})$$

To facilitate the power expansion in twist, the above amplitudes can be rewritten in terms of the conventional basis with definite twist components:

$$\begin{aligned} \psi_A(\omega, \xi) &= \frac{1}{2} (\phi_3(\omega, \xi) + \phi_4(\omega, \xi)), \\ \psi_V(\omega, \xi) &= \frac{1}{2} (-\phi_3(\omega, \xi) + \phi_4(\omega, \xi)), \\ X_A(\omega, \xi) &= \frac{1}{2} (-\phi_3(\omega, \xi) - \phi_4(\omega, \xi) + 2\psi_4(\omega, \xi)), \\ Y_A(\omega, \xi) &= \frac{1}{2} (-\phi_3(\omega, \xi) - \phi_4(\omega, \xi) + \psi_4(\omega, \xi) - \psi_5(\omega, \xi)), \\ \tilde{X}_A(\omega, \xi) &= \frac{1}{2} \left(-\phi_3(\omega, \xi) + \phi_4(\omega, \xi) - 2\tilde{\psi}_4(\omega, \xi) \right), \\ \tilde{Y}_A(\omega, \xi) &= \frac{1}{2} \left(-\phi_3(\omega, \xi) + \phi_4(\omega, \xi) - \tilde{\psi}_4(\omega, \xi) + \tilde{\psi}_5(\omega, \xi) \right), \\ W(\omega, \xi) &= \frac{1}{2} \left(\phi_4(\omega, \xi) - \psi_4(\omega, \xi) - \tilde{\psi}_4(\omega, \xi) + \phi_5(\omega, \xi) + \psi_5(\omega, \xi) + \tilde{\psi}_5(\omega, \xi) \right), \end{aligned} \quad (\text{B.4})$$

which are obtained by inverting the relations in [15].

Exponential Model

For the numerical analysis, we adopt the standard exponential model [15,33] for the B -meson LCDAs, defined as:

$$\begin{aligned} \phi_B^+(\omega) &= \frac{\omega}{\omega_0^2} e^{-\frac{\omega}{\omega_0}}, & \phi_B^-(\omega) &= \frac{1}{\omega_0} e^{-\frac{\omega}{\omega_0}}, & \phi_3(\omega, \xi) &= \frac{R-1}{(2/3)^3(1+2R)^2\omega_0} \omega \xi^2 e^{-\frac{(\omega+\xi)}{\omega_0}}, \\ \phi_4(\omega, \xi) &= \frac{R-1}{(2/3)^3(1+2R)^2} \xi^2 e^{-\frac{(\omega+\xi)}{\omega_0}}, & \psi_4(\omega, \xi) &= \frac{R}{(2/3)(1+2R)} \omega \xi e^{-\frac{(\omega+\xi)}{\omega_0}}, \\ \tilde{\psi}_4(\omega, \xi, \mu_0) &= \frac{1}{(2/3)(1+2R)} \omega \xi e^{-\frac{(\omega+\xi)}{\omega_0}}, & \psi_5(\omega, \xi, \mu_0) &= -\frac{R}{(2/3)(1+2R)\omega_0} \xi e^{-\frac{(\omega+\xi)}{\omega_0}}, \\ \tilde{\psi}_5(\omega, \xi, \mu_0) &= -\frac{1}{(2/3)(1+2R)\omega_0} \xi e^{-\frac{(\omega+\xi)}{\omega_0}}, & \phi_5(\omega, \xi, \mu_0) &= \frac{R+1}{(2/3)(1+2R)\omega_0} \omega e^{-\frac{(\omega+\xi)}{\omega_0}}, \end{aligned} \quad (\text{B.5})$$

where ω_0 in this model is equal to the inverse moment λ_B of the twist-2 DA defined as:

$$\int_0^\infty d\omega \frac{\phi_B^+(\omega)}{\omega} = \frac{1}{\lambda_B}, \quad (\text{B.6})$$

and $R \equiv \lambda_E^2/\lambda_H^2$ denotes the ratio of the chromoelectric to chromomagnetic HQET parameters. This model provides a consistent description of the two- and three-particle B -meson DAs.

C Imaginary parts of different functions

For convenience, here we collect expressions for the imaginary parts of the functions that appear in the dispersion relations of the invariant amplitudes. These equations are:

$$\begin{aligned} \operatorname{Im}\left\{\frac{1}{s-a+i\epsilon}\right\} &= -\pi\delta(s-a), \\ \operatorname{Im}\left\{\frac{1}{(s-a+i\epsilon)^n}\right\} &= \frac{(-1)^n}{(n-1)!}\pi\delta^{(n-1)}(s-a), \\ \operatorname{Im}\left\{\log(s-a+i\epsilon)\right\} &= \pi\theta(a-s), \\ \operatorname{Im}\left\{\frac{\log(s-a+i\epsilon)}{s-a+i\epsilon}\right\} &= \frac{d}{ds}(\pi\log|s-a|\Theta(a-s)), \\ \operatorname{Im}\left\{\frac{\log(s-b+i\epsilon)}{s-a+i\epsilon}\right\} &= -\pi\left(\log|s-b|\delta(s-a) - \mathcal{P}\left(\frac{1}{s-a}\right)\theta(b-s)\right), \\ \operatorname{Im}\left\{\frac{\log(s-a+i\epsilon)}{(s-a+i\epsilon)^2}\right\} &= \pi\left(\delta'(s-a) - \frac{d^2}{ds^2}(\log|s-a|\Theta(a-s))\right), \\ \operatorname{Im}\left\{\frac{\log(s-b+i\epsilon)}{(s-a+i\epsilon)^2}\right\} &= \pi\left(\mathcal{P}\left(\frac{1}{(s-a)^2}\right)\theta(b-s) + \log|s-b|\delta'(s-a)\right). \end{aligned}$$

The plus-type prescriptions entering the continuum subtraction are defined as:

$$\begin{aligned} \int_{m_s^2}^{s_0} ds \left[\frac{1}{s-a}\right]_+ g(s) &= \int_{m_s^2}^{s_0} ds \frac{1}{s-a} (g(s) - g(a)) \Theta(m_s^2 < a < s_0), \\ \int_{m_s^2}^{s_0} ds \left[\frac{1}{(s-a)^2}\right]_{++} g(s) &= \int_{m_s^2}^{s_0} ds \frac{g(s) - g(a) - (s-a)g'(a)}{(s-a)^2} \Theta(m_s^2 < a < s_0). \end{aligned}$$

These relations are employed when constructing the spectral densities $\operatorname{Im}_s I^{(X)}(q^2, s)$ from the loop amplitudes and when implementing the continuum subtraction following the quark-hadron duality ansatz.

D Expressions for invariant functions

In this appendix we provide the explicit expressions for the invariant functions $I^{(Ai)}$, $I^{(Bj)}$, and $I^{(Ck)}$ that arise from the diagrams shown in Fig. 1. These results complement the main text, where only representative examples are displayed. Throughout this appendix, whenever a coefficient function depends on the variable s , it is implicitly evaluated at the same kinematic parameter that appears in the Borel exponential that multiplies it. The relevant coefficients appearing in the invariant functions are collected in Appendix E. A prime on the coefficients indicates a derivative with respect to the dispersion variable s .

D.1 Form-factor-like contributions

For the form-factor-like diagrams (A, B), the explicit form of $I^{(A1)}$ is given in the main text. The remaining contributions read:

$$I^{(A2)}(M^2, q^2) = \frac{1}{(4\pi)^2} \left\{ \int_0^{\hat{\omega}_0} \frac{d\hat{\omega}}{(1-\hat{\omega})} \int dX \int dy_1 \frac{1}{a_s (\tilde{s}-s'_s)} \left[e^{-\tilde{s}/M^2} \left(\tilde{C}_0^{(0, \phi)} \phi_B^+(\omega) \right) \right. \right.$$

$$\begin{aligned}
& + \left(\tilde{C}_0^{(1, \Phi)} + \tilde{C}_0^{(2, \Phi)} + \tilde{C}_0^{(3, \Phi)} + 2X(y_1 \tilde{C}_1^{(5, \Phi)} + (1 - y_1) \tilde{C}_1^{(6, \Phi)}) \right) \frac{\Phi_B^\pm(\omega)}{2} \\
& \times \Theta(s_0 - \tilde{s}) - e^{-s'/M^2} \left(\tilde{C}_0^{(0, \phi)} \phi_B^+(\omega) + (\tilde{C}_0^{(1, \Phi)} + \tilde{C}_0^{(2, \Phi)} + \tilde{C}_0^{(3, \Phi)} \right. \\
& \left. + 2X(y_1 \tilde{C}_1^{(5, \Phi)} + (1 - y_1) \tilde{C}_1^{(6, \Phi)}) \frac{\Phi_B^\pm(\omega)}{2} \right) \Theta(s_0 - s'_s) \\
& + \int_0^{\hat{\omega}_0} \frac{d\hat{\omega}}{(1 - \hat{\omega})} \int dX \int dy_1 2X (\log(\tilde{a}_s X(\tilde{s} - s'_s))) e^{-\tilde{s}/M^2} (\tilde{C}_1^{(0, \phi)} \phi_B^+(\omega) \\
& + (\tilde{C}_1^{(1, \Phi)} + \tilde{C}_1^{(2, \Phi)} + \tilde{C}_1^{(3, \Phi)} + 3X(y_1 \tilde{C}_2^{(5, \Phi)} + (1 - y_1) \tilde{C}_2^{(6, \Phi)})) \frac{\Phi_B^\pm(\omega)}{2} \\
& - \int_0^{s_0} ds \int \frac{d\hat{\omega}}{(1 - \hat{\omega})} \int dX \int dy_1 2X \left[\frac{1}{s - \tilde{s}} \right]_+ \Theta(s'_s - s) e^{-s/M^2} \left(\tilde{C}_1^{(0, \phi)} \phi_B^+(\omega) \right. \\
& \left. + (\tilde{C}_1^{(1, \Phi)} + \tilde{C}_1^{(2, \Phi)} + \tilde{C}_1^{(3, \Phi)} + 3X(y_1 \tilde{C}_2^{(5, \Phi)} + (1 - y_1) \tilde{C}_2^{(6, \Phi)})) \frac{\Phi_B^\pm(\omega)}{2} \right) \\
& + \int_0^{\hat{\omega}_0} \frac{d\hat{\omega}}{(1 - \hat{\omega})^2} \int dX \int dy_1 \left(I_{\tilde{s}}^s + I_{s'}^s \right. \\
& \left. + X \frac{d}{ds} \left(\tilde{C}_1^{(4, \Phi)} e^{-s/M^2} (-1 + 2 \log(\tilde{a}_s X(s - s'_s))) \right) \Big|_{s=\tilde{s}} \right) \frac{\Phi_B^\pm(\omega)}{2} \\
& - \int_0^{s_0} ds e^{-s/M^2} \int \frac{d\hat{\omega}}{(1 - \hat{\omega})^2} \int dX \int dy_1 2X \tilde{C}_1^{(4, \Phi)} \left[\frac{1}{(s - \tilde{s})^2} \right]_{++} \Theta(s'_s - s) \frac{\Phi_B^\pm(\omega)}{2} \\
& + \int \frac{d\hat{\omega}}{(1 - \hat{\omega})} \int dX \int dy_1 \left(\frac{I_{\tilde{s}}^s}{a_s} + \frac{I_{s'}^s}{a_s} \right) (\tilde{C}_0^{(4, \Phi)} \rightarrow (y_1 \tilde{C}_0^{(5, \Phi)} + (1 - y_1) \tilde{C}_0^{(6, \Phi)}) \\
& \text{and } \tilde{s} \leftrightarrow s') \frac{\Phi_B^\pm(\omega)}{2} - \int \frac{d\hat{\omega}}{(1 - \hat{\omega})} \int dX \int dy_1 X \left(\tilde{C}_1^{(0, \phi)} \phi_B^+(\omega) + (\tilde{C}_1^{(1, \Phi)} \right. \\
& \left. + \tilde{C}_1^{(2, \Phi)} + \tilde{C}_1^{(3, \Phi)} - 5(y_1 \tilde{C}_2^{(5, \Phi)} + (1 - y_1) \tilde{C}_2^{(6, \Phi)}) e^{\frac{-\tilde{s}}{M^2}} \frac{\Phi_B^\pm(\omega)}{2} \right) \Bigg\}, \quad (\text{D.1})
\end{aligned}$$

where,

$$I_{\tilde{s}}^s = \Theta(\tilde{s} - m_s^2) \Theta(s_0 - \tilde{s}) \frac{d}{ds} \left(e^{-s/M^2} \frac{\tilde{C}_0^{(4, \Phi)}}{a_s s - S_s} \right) \Big|_{s=\tilde{s}(\omega)},$$

$$I_{s'}^s = \frac{e^{-s'/M^2}}{|a_s|} \Theta(s'_s - m_s^2) \Theta(s_0 - s'_s) \frac{\tilde{C}_0^{(4, \Phi)}}{(s'_s - \tilde{s})^2},$$

$$s'_s = \tilde{s} - \frac{1 - y_1}{y_1} (1 - \hat{\omega}) m_B^2 - \frac{X(1 - y_1)}{1 - X} \frac{q^2}{1 - \hat{\omega}},$$

$$S_s = a_s s'_s, \quad a_s = y_1 (X - 1) (1 - \hat{\omega}).$$

$$\begin{aligned}
I^{(A3)}(M^2, q^2) = & \frac{1}{(4\pi)^2} \frac{1}{m_B^2} \left\{ \int_0^{\hat{\omega}_0} d\hat{\omega} e^{\frac{-\hat{\omega}}{M^2}} \int_0^1 dx \left[\log((x^2 - x)(1 - \hat{\omega})^2 \tilde{m}_B^2) \right] \left(\frac{\tilde{A}_0^{(0,\phi)}}{(1 - \hat{\omega})^3} \phi_B^+(\omega) \right. \right. \\
& + \frac{2\tilde{A}_1^{(0,\phi)}(x^2 - x)m_B^2}{(1 - \hat{\omega})} \phi_B^+(\omega) + \frac{\tilde{A}_0^{(2,\Phi)} + \tilde{A}_0^{(3,\Phi)} + \tilde{A}_0^{(5,\Phi)}}{(1 - \hat{\omega})^3} \frac{\Phi_B^\pm(\omega)}{2} \\
& + \frac{2(\tilde{A}_1^{(2,\Phi)} + \tilde{A}_1^{(5,\Phi)})(x^2 - x)m_B^2}{(1 - \hat{\omega})} \frac{\Phi_B^\pm(\omega)}{2} + \left(-\frac{1}{M^2} \frac{\tilde{A}_0^{(4,\Phi)}}{(1 - \hat{\omega})^4} + \frac{\tilde{A}_0'^{(4,\Phi)}}{(1 - \hat{\omega})^4} \right) \frac{\Phi_B^\pm(\omega)}{2} \\
& + \left(-\frac{1}{M^2} \frac{\tilde{A}_1^{(4,\Phi)}}{(1 - \hat{\omega})^2} + \frac{\tilde{A}_1'^{(4,\Phi)}}{(1 - \hat{\omega})^2} \right) 2(x^2 - x)m_B^2 \frac{\Phi_B^\pm(\omega)}{2} + 2x \frac{\tilde{A}_1^{(6,\Phi)}}{(1 - \hat{\omega})^3} \frac{\Phi_B^\pm(\omega)}{2} \\
& - \frac{1}{1 - x} \frac{\tilde{A}_0^{(6,\Phi)}}{(1 - \hat{\omega})^5 m_B^2} \frac{\Phi_B^\pm(\omega)}{2} - \frac{1}{(1 - \hat{\omega})} \left(\left(\tilde{A}_1^{(0,\phi)} \phi_B^+(\omega) + (\tilde{A}_1^{(2,\Phi)} + \tilde{A}_1^{(5,\Phi)} + \frac{x\tilde{A}_1^{(6,\Phi)}}{(1 - \hat{\omega})^2}) \right. \right. \\
& \left. \left. \times \frac{\Phi_B^\pm(\omega)}{2} \right) (x^2 - x)m_B^2 \right) - \left(-\frac{1}{M^2} \frac{\tilde{A}_1^{(4,\Phi)}}{(1 - \hat{\omega})^2} + \frac{\tilde{A}_1'^{(4,\Phi)}}{(1 - \hat{\omega})^2} \right) (x^2 - x)m_B^2 \frac{\Phi_B^\pm(\omega)}{2} \left. \right\}, \tag{D.2}
\end{aligned}$$

$$\begin{aligned}
I^{(B1)}(M^2, q^2) = & \frac{-1}{(4\pi)^2} \frac{1}{m_b^2} \int_0^{\hat{\omega}_0} d\hat{\omega} e^{\frac{-\hat{\omega}}{M^2}} \frac{1}{(1 - \hat{\omega})} \int_0^1 dx \\
& \left\{ \left[\left(\bar{A}_0^{(0,\phi)} + 2\bar{A}_1^{(0,\phi)} m_b^2 \right) \phi_B^+(\omega) + \left(\bar{A}_0^{(1,\Phi)} + 2\bar{A}_1^{(1,\Phi)} m_b^2 + \left(-\frac{\bar{A}_0^{(2,\Phi)}}{(1 - \hat{\omega})M^2} \right. \right. \right. \\
& + \left. \left. \frac{\bar{A}_0'^{(2,\Phi)}}{(1 - \hat{\omega})} \right) + 2 \left(-\frac{\bar{A}_1^{(2,\Phi)}}{(1 - \hat{\omega})M^2} + \frac{\bar{A}_1'^{(2,\Phi)}}{(1 - \hat{\omega})} \right) m_b^2 \right] \frac{\Phi_B^\pm(\omega)}{2} \right] \log(\tilde{m}_b^2) \\
& - \left(\bar{A}_1^{(0,\phi)} \phi_B^+(\omega) + (\bar{A}_1^{(1,\Phi)} - \frac{\bar{A}_1^{(2,\Phi)}}{(1 - \hat{\omega})M^2} + \frac{\bar{A}_1'^{(2,\Phi)}}{(1 - \hat{\omega})}) \frac{\Phi_B^\pm(\omega)}{2} \right) m_b^2 \left. \right\}, \tag{D.3}
\end{aligned}$$

$$\begin{aligned}
I^{(B2)}(M^2, q^2) = & \frac{1}{(4\pi)^2} \left\{ \int_0^{\hat{\omega}_0} \frac{d\hat{\omega}}{(1 - \hat{\omega})} \int dX \int dy_1 \left[\frac{1}{a_b (\tilde{s} - s'_b)} \left(e^{-\tilde{s}/M^2} \left(\bar{C}_0^{(0,\phi)} \phi_B^+(\omega) \right. \right. \right. \\
& + \left. \left. \bar{C}_0^{(1,\Phi)} \frac{\Phi_B^\pm(\omega)}{2} \right) \Theta(s_0 - s'_b) - e^{-s'_b/M^2} \left(\bar{C}_0^{(0,\phi)} \phi_B^+(\omega) + \bar{C}_0^{(1,\Phi)} \frac{\Phi_B^\pm(\omega)}{2} \right) \Theta(s_0 - s'_b) \right) \\
& + X(-1 + 2 \log(\tilde{a}_b X(\tilde{s} - s'_b))) \left(\bar{C}_1^{(0,\phi)} \phi_B^+(\omega) + \bar{C}_1^{(1,\Phi)} \frac{\Phi_B^\pm(\omega)}{2} \right) \left. \right] \\
& - \int_0^{s_0} ds \int \frac{d\hat{\omega}}{(1 - \hat{\omega})} \int dX \int dy_1 e^{\frac{-\hat{\omega}}{M^2}} 2X \Theta(s' - s) \left[\frac{1}{s - \tilde{s}} \right]_+ \left(\bar{C}_1^{(0,\phi)} \phi_B^+(\omega) \right. \\
& \left. + \bar{C}_1^{(1,\Phi)} \frac{\Phi_B^\pm(\omega)}{2} \right) + \int_0^{\hat{\omega}_0} \frac{d\hat{\omega}}{(1 - \hat{\omega})^2} \int dX \int dy_1 \frac{\Phi_B^\pm(\omega)}{2} \left(I_{\tilde{s}}^b + I_{s'}^b \right)
\end{aligned}$$

$$\begin{aligned}
& - X \frac{d}{ds} \left(\bar{C}_1^{(2, \Phi)} e^{-s/M^2} \right) \Big|_{s=\tilde{s}} + 2X \frac{d}{ds} \left(\bar{C}_1^{(2, \Phi)} e^{-s/M^2} \log(\tilde{a}_b X(s-s')) \right) \Big|_{s=\tilde{s}} \\
& - \int_0^{s_0} ds e^{-s/M^2} \int \frac{d\hat{\omega}}{(1-\hat{\omega})^2} \int dX \int dy_1 2X \bar{C}_1^{(2, \Phi)} \Theta(s'-s) \left[\frac{1}{(s-\tilde{s})^2} \right]_{++} \frac{\Phi_B^\pm}{2} \Bigg\}, \tag{D.4}
\end{aligned}$$

with:

$$I_{\tilde{s}}^b = \Theta(\tilde{s} - m_s^2) \Theta(s_0 - \tilde{s}) \frac{d}{ds} \left(e^{-s/M^2} \frac{\bar{C}_0^{(2, \phi)}}{a_b s - S_b} \right) \Big|_{s=\tilde{s}(\omega)},$$

$$I_{s'}^b = \frac{e^{-s'_b/M^2}}{|a_b|} \Theta(s'_b - m_s^2) \Theta(s_0 - s'_b) \frac{\bar{C}_0^{(2, \phi)}}{(s'_b - \tilde{s})^2},$$

$$s'_b = m_B^2 \hat{m}_b (\hat{m}_b (1 - y_1 - X) + (1 - y_1)(X - 2)) + (1 - y_1) q^2 (\hat{m}_b (X - 1) - X(1 - y_1) + 1),$$

$$S_b = a_b s'_b, \quad a_b = \hat{m}_b (1 - y_1)(X - 1).$$

$$\begin{aligned}
I^{(B3)}(M^2, q^2) &= \frac{-1}{(4\pi)^2} \frac{1}{m_B^2} \int_0^{\hat{\omega}_0} d\hat{\omega} e^{-\frac{\tilde{s}}{M^2}} \frac{1}{(1-\hat{\omega})^3} \int dx \\
& \left[-(\bar{B}_0^{(0, \phi)} + 2\bar{B}_1^{(0, \phi)} x^2 m_b^2) \log(x^2 \tilde{m}_b^2) \phi_B^+(\omega) - \left(\bar{B}_0^{(1, \Phi)} + \bar{B}_0^{(2, \Phi)} \right. \right. \\
& + \left(-\frac{\bar{B}_0^{(3, \Phi)}}{(1-\hat{\omega})M^2} + \frac{\bar{B}'_0^{(3, \Phi)}}{(1-\hat{\omega})} \right) + \frac{\bar{B}_0^{(4, \Phi)}}{(1-\hat{\omega})^2 m_B^2} + \left(\bar{B}_1^{(1, \Phi)} + \bar{B}_1^{(2, \Phi)} + \right. \\
& + \left. \left. \left(-\frac{\bar{B}_1^{(3, \Phi)}}{(1-\hat{\omega})M^2} + \frac{\bar{B}'_1^{(3, \Phi)}}{(1-\hat{\omega})} \right) + \frac{\bar{B}_1^{(4, \Phi)}}{(1-\hat{\omega})^2 m_B^2} \right) x^2 m_b^2 \right) \log(x^2 \tilde{m}_b^2) \frac{\Phi_B^\pm(\omega)}{2} \\
& + \left(\bar{B}_1^{(0, \phi)} \phi_B^+(\omega) + (\bar{B}_1^{(1, \Phi)} + \bar{B}_1^{(2, \Phi)} - \frac{\bar{B}_1^{(3, \Phi)}}{(1-\hat{\omega})M^2} + \frac{\bar{B}'_1^{(3, \Phi)}}{(1-\hat{\omega})} \right. \\
& \left. \left. + \frac{\bar{B}_1^{(4, \Phi)}}{(1-\hat{\omega})^2 m_B^2} \right) \frac{\Phi_B^\pm(\omega)}{2} \right] x^2 m_b^2. \tag{D.5}
\end{aligned}$$

D.2 Hard-scattering contributions

For the hard-scattering diagrams (C), the explicit form of $I^{(C1)}$ is given in the main text. The remaining contributions read:

$$\begin{aligned}
I^{(C2)}(M^2, q^2) &= \frac{-1}{(4\pi)^2} \int_{m_s^2}^{s_0} ds e^{-s/M^2} \int_0^\infty d\omega \int_0^1 dX \int_0^1 dy_1 \int_0^1 dy_2 (1 - y_1) \\
& \left\{ \left(\frac{-1}{M^2} B_0^{(0, \phi)}(\omega, X, y_1, y_2, s, q^2) + B_0'^{(0, \phi)}(\omega, X, y_1, y_2, q^2) \right. \right. \\
& \left. \left. - 2X B_1^{(0, \phi)}(\omega, X, y_1, y_2, s, q^2) \right) \frac{\delta(\mathcal{W}_{C2} s - \mathcal{X}_{C2})}{\mathcal{W}_{C2}} \phi_B^+(\omega) \right.
\end{aligned}$$

$$\begin{aligned}
& + \left(- \frac{(B_0^{(1,\Phi)} + B_0^{(2,\Phi)} + B_0^{(3,\Phi)})}{M^2} + (B_0'^{(1,\Phi)} + B_0'^{(2,\Phi)} + B_0'^{(3,\Phi)}) \right. \\
& - 2X (B_1^{(1,\Phi)} + B_1^{(2,\Phi)} + B_1^{(3,\Phi)}) + \frac{1}{M^4} (y_1 B_0^{(4,\Phi)} + (1-y_1) B_0^{(5,\Phi)}) \\
& + (1-y_1)(1-y_2) B_0^{(6,\Phi)} - \frac{1}{M^2} 2(y_1 B_0'^{(4,\Phi)} + (1-y_1) B_0'^{(5,\Phi)} + (1-y_1) \\
& \quad \times (1-y_2) B_0'^{(6,\Phi)}) + (y_1 B_0''^{(4,\Phi)} + (1-y_1) B_0''^{(5,\Phi)} + (1-y_1)(1-y_2) B_0''^{(6,\Phi)}) \\
& \left. - \frac{2X (y_1 B_1^{(4,\Phi)} + (1-y_1) B_1^{(5,\Phi)} + (1-y_1)(1-y_2) B_1^{(6,\Phi)})}{M^2} \right. \\
& + 2X (y_1 B_1'^{(4,\Phi)} + (1-y_1) B_1'^{(5,\Phi)} + (1-y_1)(1-y_2) B_1'^{(6,\Phi)}) + 6X^2 (y_1 B_2^{(4,\Phi)} \\
& \left. + (1-y_1) B_2^{(5,\Phi)} + (1-y_1)(1-y_2) B_2^{(6,\Phi)}) \right) \frac{\delta(\mathcal{W}_{C_2} s - \mathcal{X}_{C_2})}{\mathcal{W}_{C_2}} \frac{\Phi_B^\pm(\omega)}{2} \Bigg\}, \tag{D.6}
\end{aligned}$$

where

$$\begin{aligned}
(\mathcal{W}_{C_2} s - \mathcal{X}_{C_2}) = & - \left[y_2 \bar{y}_1 (1 - \omega - X(1 - \omega - y_1)) s \right. \\
& \left. + (\bar{X} \bar{y}_1 \omega (q^2 y_2 - m_B^2 (1 + \bar{y}_2)) + \bar{y}_1 \bar{y}_2 (m_B^2 - m_B^2 X \bar{y}_1 + q^2 X \bar{y}_1 y_2) + m_B^2 \omega^2 \bar{X}) \right].
\end{aligned}$$

$$\begin{aligned}
I^{(C_3)}(M^2, q^2) = & \frac{-1}{(4\pi)^2} \int_{m_s^2}^{s_0} ds e^{-s/M^2} \int_0^\infty d\omega \int_0^1 dX \int_0^1 dy_1 \int_0^1 dy_2 (1-y_1) \\
& \left\{ \left(\frac{-1}{M^2} A_0^{(0,\phi)}(\omega, X, y_1, y_2, s, q^2) + A_0'^{(0,\phi)}(\omega, X, y_1, y_2, q^2) \right. \right. \\
& \left. \left. - 2X A_1^{(0,\phi)}(\omega, X, y_1, y_2, s, q^2) \right) \frac{\delta(\mathcal{W}_{C_3} s - \mathcal{X}_{C_3})}{\mathcal{W}_{C_3}} \phi_B^+(\omega) \right. \\
& + \left(- \frac{(A_0^{(1,\Phi)} + A_0^{(2,\Phi)} + A_0^{(3,\Phi)})}{M^2} + (A_0'^{(1,\Phi)} + A_0'^{(2,\Phi)} + A_0'^{(3,\Phi)}) \right. \\
& - 2X (A_1^{(1,\Phi)} + A_1^{(2,\Phi)} + A_1^{(3,\Phi)}) + \frac{(y_1 A_0^{(4,\Phi)} + (1-y_1) A_0^{(5,\Phi)} + (1-y_1)(1-y_2) A_0^{(6,\Phi)})}{M^4} \\
& \left. - \frac{2(y_1 A_0'^{(4,\Phi)} + (1-y_1) A_0'^{(5,\Phi)} + (1-y_1)(1-y_2) A_0'^{(6,\Phi)})}{M^2} \right. \\
& + (y_1 A_0''^{(4,\Phi)} + (1-y_1) A_0''^{(5,\Phi)} + (1-y_1)(1-y_2) A_0''^{(6,\Phi)}) \\
& \left. - \frac{2X (y_1 A_1^{(4,\Phi)} + (1-y_1) A_1^{(5,\Phi)} + (1-y_1)(1-y_2) A_1^{(6,\Phi)})}{M^2} \right. \\
& \left. + 2X (y_1 A_1'^{(4,\Phi)} + (1-y_1) A_1'^{(5,\Phi)} + (1-y_1)(1-y_2) A_1'^{(6,\Phi)}) + 6X^2 (y_1 A_2^{(4,\Phi)} \right.
\end{aligned}$$

$$+ (1 - y_1)A_2^{(5,\Phi)} + (1 - y_1)(1 - y_2)A_2^{(6,\Phi)} \left. \frac{\delta(\mathcal{W}_{C3} s - \mathcal{X}_{C3})}{\mathcal{W}_{C3}} \frac{\Phi_B^\pm(\omega)}{2} \right\}, \quad (\text{D.7})$$

where

$$\begin{aligned} \mathcal{W}_{C3} s - \mathcal{X}_{C3} = & m_B^2 \left[-((1 - X \bar{y}_1) \bar{y}_1 \bar{y}_2) - \bar{X} \bar{y}_1 (-2 + y_2) \omega - \bar{X} \omega^2 \right] \\ & - \bar{y}_1 y_2 \left[q^2 + s X \bar{y}_1 \bar{y}_2 - q^2 \omega + s \bar{X} \omega + q^2 X (-\bar{y}_1 + \omega) \right]. \end{aligned}$$

$$\begin{aligned} I^{(C4)}(M^2, q^2) = & \int_{m_s^2}^{s_0} ds e^{-s/M^2} \int_0^\infty d\omega \int_0^1 dX dy_1 \frac{1}{\hat{\omega}(s - a_{C4}(q^2, \omega))} \\ & \left\{ \left(\frac{C_0^{(0,\phi)}}{\mathcal{W}_{C4}} \delta(\mathcal{W}_{C4} s - \mathcal{X}_{C4}) - 2X C_1^{(0,\phi)} \Theta(\mathcal{X}_{C4} - \mathcal{W}_{C4} s) \right) \phi_B^+(\omega) \right. \\ & + \left(\left((C_0^{(1,\Phi)} + C_0^{(2,\Phi)} + C_0^{(3,\Phi)}) + \frac{C_0^{(4,\Phi)}}{\hat{\omega}(s - a_{C4}(q^2, \omega))} + \frac{(y_1 C_0^{(5,\Phi)} + (1 - y_1) C_0^{(6,\Phi)})}{M^2} \right. \right. \\ & - (y_1 C_0'^{(5,\Phi)} + (1 - y_1) C_0'^{(6,\Phi)}) + 2X (y_1 C_1^{(5,\Phi)} + (1 - y_1) C_1^{(6,\Phi)}) \left. \left. \right) \frac{\delta(\mathcal{W}_{C4} s - \mathcal{X}_{C4})}{\mathcal{W}_{C4}} \right. \\ & - 2X \left(C_1^{(1,\Phi)} + C_1^{(2,\Phi)} + C_1^{(3,\Phi)} + \frac{C_1^{(4,\Phi)}}{\hat{\omega}(s - a(q^2, \omega))} + 3X (y_1 C_2^{(5,\Phi)} \right. \\ & \left. \left. + (1 - y_1) C_2^{(6,\Phi)}) \right) \Theta(\mathcal{X}_{C4} - \mathcal{W}_{C4} s) \right) \frac{\Phi_B^\pm(\omega)}{2} \left. \right\}, \quad (\text{D.8}) \end{aligned}$$

where

$$\mathcal{W}_{C4} s - \mathcal{X}_{C4} = -y_1(\omega \bar{X} + X \bar{y}_1) s - \bar{X} \bar{\omega} (q^2 y_1 - m_B^2 (\omega - \bar{y}_1)).$$

D.3 Soft-gluon contribution

For the soft-gluon diagrams (D), the explicit form of $I^{(D1)}$ is given in the main text. The remaining contributions read:

$$\begin{aligned} I^{(D2)}(p^2, q^2) = & \sum_{n=1,2} \int_0^\infty d\omega \int_0^\infty d\xi \frac{1}{[(\omega v - p)^2]^n} \left[\tilde{F}_n^{(\Psi_{AV})}(q^2, \omega) (\Psi_A(\omega, \xi) - \Psi_V(\omega, \xi)) \right. \\ & + \tilde{F}_n^{(\Psi_V)}(q^2, \omega) \Psi_V(\omega, \xi) + \tilde{F}_n^{(X_A)}(q^2, \omega) \bar{X}_A(\omega, \xi) + \tilde{F}_n^{(W_{YA})}(q^2, \omega) (\bar{W}(\omega, \xi) \\ & \left. + \bar{Y}_A(\omega, \xi)) + \tilde{F}_n^{(\bar{X}_A)}(q^2, \omega) \bar{\bar{X}}_A(\omega, \xi) + \tilde{F}_n^{(\bar{Y}_A)}(q^2, \omega) \bar{\bar{Y}}_A(\omega, \xi) \right]. \quad (\text{D.9}) \end{aligned}$$

These contributions are expressed in terms of three-particle B -meson DAs and the coefficient functions defined in Appendix B and E.

E Coefficients in the LCSR integrals

This appendix collects the explicit expressions of the coefficient functions $\tilde{B}_i^{(j,\phi/\Phi)}$, $D_i^{(j,\phi/\Phi)}$, and $F_n^{(X)}$ that enter the invariant amplitudes $I^{(A1)}$, $I^{(C1)}$, and $I^{(D1)}$, respectively. The full set of coefficients used in the diagrams of Fig. 1 are given in the ancillary file accompanying this paper. All coefficients depend on the external and kinematic variables as

$$\tilde{X}_i^{(j,\phi/\Phi)} = \tilde{X}_i^{(j,\phi/\Phi)}(s, q^2, m_B, m_b, \hat{\omega}; x \text{ or } x_2, x_3), \quad \hat{m}_b = m_b/m_B, \quad \hat{\omega} = \omega/m_B.$$

The superscript $\phi(\Phi)$ denotes the terms multiplying the twist-2(3) B -meson distribution amplitudes defined in Appendix B. In the analytical expressions presented in this appendix, the strange-quark mass m_s is omitted for brevity; however, it is considered in our numerical evaluations.

E.1 Coefficients $\tilde{B}_i^{(j,\phi/\Phi)}$

The coefficients used in the $I^{(A1)}$ function (\tilde{B}) are given below:

$$\begin{aligned} \tilde{B}_0^{(0,\phi)} = & 4 m_B (2\hat{m}_b - 1) (x - 1) x (\hat{\omega} - 1) [(\hat{\omega} - 1)(2\hat{\omega} - 5) s + ((3 - 2\hat{\omega})\hat{\omega} + 2) q^2 \\ & + m_B^2 (\hat{\omega}^2 + \hat{\omega} - 2)], \end{aligned}$$

$$\tilde{B}_1^{(0,\phi)} = 12 m_B (2\hat{m}_b - 1) (\hat{\omega} - 1),$$

$$\begin{aligned} \tilde{B}_0^{(1,\Phi)} = & - 8 (x - 1) x [(\hat{\omega} - 1) s (2\hat{m}_b(\hat{\omega} - 4) - 2\hat{\omega} + 5) + q^2 (- 2\hat{m}_b(\hat{\omega} - 2)\hat{\omega} + 4\hat{m}_b - 3) \\ & + m_B^2 (\hat{\omega} - 1) (4\hat{m}_b\hat{\omega} + 2\hat{m}_b - \hat{\omega} - 2)], \end{aligned}$$

$$\tilde{B}_1^{(1,\Phi)} = - 24 (2\hat{m}_b - 1),$$

$$\begin{aligned} \tilde{B}_0^{(2,\Phi)} = & - 8 x [- (2\hat{m}_b + 1)(\hat{\omega} - 1) s + q^2 (2\hat{m}_b(\hat{\omega} - 2) - 3\hat{\omega} + 4) + m_B^2 (\hat{\omega} - 1) \\ & (6\hat{m}_b\hat{\omega} - 4\hat{m}_b - 3\hat{\omega} + 4)], \end{aligned}$$

$$\tilde{B}_1^{(2,\Phi)} = 0,$$

$$\begin{aligned} \tilde{B}_0^{(3,\Phi)} = & - 8 (x - 1) x \left\{ - (\hat{\omega} - 1) q^2 [s (2\hat{m}_b(\hat{\omega} - 4) - 5\hat{\omega} + 11) + m_B^2 (2\hat{m}_b (2(\hat{\omega} - 2)\hat{\omega}^2 + \hat{\omega} + 4) \right. \\ & + \hat{\omega} ((7 - 2\hat{\omega})\hat{\omega} - 3) - 8)] + (\hat{\omega} - 1)^2 s [(5 - 2\hat{\omega}) s + 2m_B^2 (\hat{m}_b(\hat{\omega} - 1)(2\hat{\omega} - 5) \\ & - (\hat{\omega} - 4)\hat{\omega} - 6)] + q^4 (2\hat{m}_b((\hat{\omega} - 2)\hat{\omega} - 2) + \hat{\omega} (2(\hat{\omega} - 3)\hat{\omega} + 3) + 4) \\ & \left. + m_B^4 (\hat{\omega} - 1)^2 (\hat{\omega} + 2) (2\hat{m}_b(\hat{\omega} - 1) - \hat{\omega} + 2) \right\}, \end{aligned}$$

$$\tilde{B}_1^{(3,\Phi)} = - 24 [- q^2 (2\hat{m}_b + \hat{\omega} - 2) - (\hat{\omega} - 1) s + m_B^2 (\hat{\omega} - 1) (2\hat{m}_b(\hat{\omega} - 1) - \hat{\omega} + 2)],$$

$$\tilde{B}_0^{(4,\Phi)} = 8 (x - 1)^2 x \left\{ - (\hat{\omega} - 2)(\hat{\omega} - 1) q^2 [s (- 2\hat{m}_b(\hat{\omega} - 4) + 5\hat{\omega} - 11) \right.$$

$$\begin{aligned}
& + m_B^2 (2\hat{m}_b((\hat{\omega} - 1)\hat{\omega} - 3) + (3 - 4\hat{\omega})\hat{\omega} + 7)] + (\hat{\omega} - 1)^2 s [(\hat{\omega} - 2)(2\hat{\omega} - 5) s \\
& + m_B^2 (2\hat{m}_b(\hat{\omega} - 1)(2\hat{\omega} - 5) + (16 - 3\hat{\omega})\hat{\omega} - 19)] - (\hat{\omega} - 2) q^4 (2\hat{m}_b((\hat{\omega} - 2)\hat{\omega} - 2) \\
& + \hat{\omega}(2(\hat{\omega} - 3)\hat{\omega} + 3) + 4) + m_B^4 (\hat{\omega} - 1)^2 (\hat{\omega} + 2) (2\hat{m}_b(\hat{\omega} - 1) - 2\hat{\omega} + 3) \Big\},
\end{aligned}$$

$$\begin{aligned}
\tilde{B}_1^{(4,\Phi)} = & 4 \Big\{ - (\hat{\omega} - 1) s (\hat{\omega} (3\hat{m}_b(x - 1) - 5x + 7) + 4\hat{m}_b + 14x - 15) \\
& + q^2 (\hat{\omega}^2 (3\hat{m}_b(x - 1) + 5x - 3) + \hat{\omega} (\hat{m}_b(11x - 7) - 21x + 18) - 26\hat{m}_b x + 24\hat{m}_b \\
& + 25x - 23) + m_B^2 (\hat{\omega} - 1) (\hat{m}_b (3x(7\hat{\omega} - 6) - 15\hat{\omega} + 16) - 14x\hat{\omega} + 23x + 13\hat{\omega} - 21) \\
& - 2(\hat{m}_b(\hat{\omega} (2(x - 1)\hat{\omega} + x + 3) - 2) + x\hat{\omega}(4\hat{\omega} - 5) + x - \hat{\omega} + 1) \Big\}.
\end{aligned}$$

E.2 Coefficients $D_i^{(j,\phi/\Phi)}$

The coefficients used in the $I^{(C1)}$ function (D) are given below:

$$\begin{aligned}
D_0^{(0,\phi)}(s, q^2) = & - 4 m_B \Big(\hat{\omega} \left(x_3 q^2 [\hat{\omega}(x_2 + x_3 - 1)(6\hat{m}_b(x_2 + x_3 - 1) - 3x_2 - 3x_3 + 4) \right. \\
& - (x_3 - 1)((6\hat{m}_b - 3)x_2 + 6\hat{m}_b x_3 - 3x_3 + 1)] + m_B^2 [3(2\hat{m}_b - 1)\hat{\omega}^2 \\
& (x_2 + x_3 - 1)^2 (x_2 + x_3) - \hat{\omega}(x_2 + x_3 - 1)(3(2\hat{m}_b - 1)x_2(2x_3 - 1) \\
& + 2x_3(6\hat{m}_b x_3 - 3\hat{m}_b - 3x_3 + 2)) + (x_3 - 1)x_3((6\hat{m}_b - 3)x_2 + 6\hat{m}_b x_3 \\
& \left. - 3x_3 + 1) \right] \Big) - x_3 s (\hat{\omega}(x_2 + x_3 - 1) - x_3 + 1) (\hat{\omega}(6\hat{m}_b(x_2 - 1) - 3x_2 \\
& + 2) + 3(2\hat{m}_b - 1)x_3(\hat{\omega} - 1)),
\end{aligned}$$

$$D_1^{(0,\phi)}(s, q^2) = - 6 m_B (2\hat{m}_b - 1) ((3x_2 - 4)\hat{\omega} + 3x_3(\hat{\omega} - 1) + 2),$$

$$D_2^{(0,\phi)}(s, q^2) = 0,$$

$$\begin{aligned}
D_0^{(1,\phi)}(s, q^2) = & 8 \Big(- (4\hat{m}_b - 1) x_3 s (\hat{\omega}(x_2 + x_3 - 1) - x_3 + 1) + x_3 q^2 ((4\hat{m}_b - 3)\hat{\omega}(x_2 + x_3 - 1) \\
& - 2(\hat{m}_b - 1)(x_3 - 1)) + m_B^2 (\hat{\omega}(x_2 + x_3 - 1) - x_3 + 1) (3(2\hat{m}_b - 1)\hat{\omega}(x_2 + x_3) \\
& - 2(\hat{m}_b - 1)x_3) \Big),
\end{aligned}$$

$$D_1^{(1,\phi)}(s, q^2) = 12 (2\hat{m}_b - 1),$$

$$D_2^{(1,\phi)}(s, q^2) = 0,$$

$$D_0^{(2,\phi)}(s, q^2) = 24 \Big(x_3 s (\hat{\omega}(-2\hat{m}_b x_2 + 2\hat{m}_b + x_2) + x_3(-2\hat{m}_b \hat{\omega} + 2\hat{m}_b + \hat{\omega} - 1)) + x_3 \hat{\omega} q^2 (2\hat{m}_b(x_2$$

$$\begin{aligned}
& + x_3 - 1) - x_2 - x_3 + 2) + m_B^2 \hat{\omega} \left((2\hat{m}_b - 1) \hat{\omega} (x_2 + x_3 - 1)(x_2 + x_3) \right. \\
& \left. + x_3(-2\hat{m}_b x_2 - 2\hat{m}_b x_3 + x_2 + x_3 - 1) \right),
\end{aligned}$$

$$D_1^{(2,\phi)}(s, q^2) = 24(2\hat{m}_b - 1),$$

$$D_2^{(2,\phi)}(s, q^2) = 0,$$

$$\begin{aligned}
D_0^{(3,\phi)}(s, q^2) = & -8 \left(x_3 s \left[x_3 q^2 \left(\hat{\omega} (2\hat{m}_b (5x_2 x_3 - 3x_2 + 5x_3^2 - 7x_3 + 2) - 6x_3 (x_2 + x_3) + 3x_2 + 10x_3 - 4) \right. \right. \right. \\
& - 4(2\hat{m}_b - 1) \hat{\omega}^2 (x_2 + x_3 - 1)^2 - 2(\hat{m}_b - 1)(x_3 - 1)x_3) - 2m_B^2 (\hat{\omega} (x_2 + x_3 - 1) - x_3 \\
& + 1) \left(\hat{\omega}^2 (x_2 + x_3 - 1) (\hat{m}_b (5x_2 + 5x_3 - 3) - 2x_2 - 2x_3 + 1) + x_3 \hat{\omega} (\hat{m}_b (-6x_2 - 6x_3 + 4) \right. \\
& \left. \left. + 3(x_2 + x_3 - 1) + (\hat{m}_b - 1)x_3^2) \right] + \hat{\omega} \left[x_3 q^2 \left(x_3 q^2 (\hat{\omega} (x_2 + x_3 - 1) (4\hat{m}_b (x_2 + x_3 - 1) \right. \right. \right. \\
& - 3x_2 - 3x_3 + 4) - 2(\hat{m}_b - 1)(x_3 - 1)(x_2 + x_3)) + m_B^2 \left(2\hat{\omega}^2 (x_2 + x_3 - 1)^2 (\hat{m}_b (5x_2 \right. \\
& + 5x_3 - 3) - 3x_2 - 3x_3 + 2) - \hat{\omega} (x_2 + x_3 - 1) \left(x_2 (2(7\hat{m}_b - 5)x_3 - 8\hat{m}_b + 5) \right. \\
& \left. \left. + 2x_3 (7\hat{m}_b x_3 - 6\hat{m}_b - 5x_3 + 5) - 1) \right) + 4(\hat{m}_b - 1)(x_3 - 1)x_3 (x_2 + x_3) \right] \right) \\
& + m_B^4 (\hat{\omega} (x_2 + x_3 - 1) - x_3 + 1) \left(2(\hat{m}_b - 1)x_3^2 (x_2 + x_3) + 3(2\hat{m}_b - 1) \hat{\omega}^2 (x_2 + x_3 - 1)^2 \right. \\
& \left. (x_2 + x_3) - x_3 \hat{\omega} (x_2 + x_3 - 1) ((8\hat{m}_b - 5)x_2 + 8\hat{m}_b x_3 - 5x_3 + 1) \right) \left. \right] + x_3^2 s^2 \\
& \left(\hat{\omega} (x_2 + x_3 - 1) - x_3 + 1) (4\hat{m}_b (x_2 - 1) \hat{\omega} + (4\hat{m}_b - 1)x_3 (\hat{\omega} - 1) - x_2 \hat{\omega}) \right),
\end{aligned}$$

$$\begin{aligned}
D_1^{(3,\phi)}(s, q^2) = & -4 \left(-s \left(x_3 (\hat{m}_b (16x_2 \hat{\omega} - 15\hat{\omega} + 7) + \hat{\omega} (2x_2 (\hat{\omega} - 3) - 3\hat{\omega} + 3) - 2) \right. \right. \\
& \left. \left. + (x_2 - 2) \hat{\omega} (\hat{m}_b + (x_2 - 1) \hat{\omega} + 1) + x_3^2 (\hat{\omega} - 1) (16\hat{m}_b + \hat{\omega} - 5) \right) \right. \\
& \left. + q^2 \left(\hat{\omega} (\hat{m}_b (16x_2 x_3 + x_2 + x_3 (16x_3 - 15)) - 2) - 12x_3 (x_2 + x_3) + x_2 + 15x_3 + 2) \right. \right. \\
& \left. \left. - 3(\hat{m}_b - 1)x_3 (2x_3 - 1) + \hat{\omega}^2 (x_2 + x_3 - 2)(x_2 + x_3 - 1) \right) + 2\hat{\omega}^2 (x_2 + x_3 - 1) \right. \\
& \left(m_B^2 (\hat{m}_b (11x_2 + 11x_3 - 8) - 5x_2 - 5x_3 + 3) + 2(8\hat{m}_b (x_2 + x_3 - 1) - 5x_2 \right. \\
& \left. - 5x_3 + 6) \right) + \hat{\omega} \left(-\hat{m}_b (m_B^2 (x_2 (28x_3 - 11) + x_3 (28x_3 - 33) + 6) + 40x_3 (x_2 + x_3) \right. \\
& \left. - 4(7x_2 + 15x_3 - 6)) + m_B^2 (4x_2 (4x_3 - 1) + x_3 (16x_3 - 21)) + 26x_3 (x_2 + x_3) \right. \\
& \left. \left. - 20x_2 - 42x_3 + 20) + x_3 (3m_B^2 (\hat{m}_b - 1)(2x_3 - 1) + 2\hat{m}_b (6x_3 - 7) - 8x_3 + 10) \right) \right),
\end{aligned}$$

$$D_2^{(3,\phi)}(s, q^2) = -12(2\hat{m}_b - 1),$$

$$\begin{aligned} D_0^{(4,\phi)}(s, q^2) = & 8 \left(s \left((x_3 - 1)x_3 q^2 (4(2\hat{m}_b - 1)\hat{\omega}^2(x_2 + x_3 - 1)^2 + \hat{\omega}(2\hat{m}_b(x_2(3 - 5x_3) \right. \right. \\ & + (7 - 5x_3)x_3 - 2) + 6x_3(x_2 + x_3) - 3x_2 - 10x_3 + 4) + 2(\hat{m}_b - 1)(x_3 - 1)x_3) \\ & + m_B^2 (\hat{\omega}(x_2 + x_3 - 1) - x_3 + 1) \left[x_3 \hat{\omega} (3(2x_3 - 1)(x_2 + x_3 - 1) - 2\hat{m}_b(6x_2x_3 \right. \\ & - 3x_2 + 6x_3^2 - 7x_3 + 1)) + \hat{\omega}^2(x_2 + x_3 - 1)(x_2(10\hat{m}_b x_3 - 4\hat{m}_b - 4x_3 + 1) \\ & + x_3(10\hat{m}_b(x_3 - 1) - 4x_3 + 3)) + 2(\hat{m}_b - 1)(x_3 - 1)x_3^2 \left. \right] + \hat{\omega} \left(m_B^2 q^2 \left[-\hat{\omega}^2 \right. \right. \\ & (x_2 + x_3 - 1)^2 (x_2(10\hat{m}_b x_3 - 4\hat{m}_b - 6x_3 + 3) + x_3(10\hat{m}_b(x_3 - 1) - 6x_3 + 7)) \\ & + (x_3 - 1)\hat{\omega}(x_2 + x_3 - 1) \left(2x_2(7\hat{m}_b x_3 - \hat{m}_b - 5x_3 + 1) + x_3(2(7\hat{m}_b - 5)x_3 - 6\hat{m}_b + 7) \right) \\ & - 4(\hat{m}_b - 1)x_3(x_3 - 1)^2(x_2 + x_3) \left. \right] - (x_3 - 1)x_3 q^4 (\hat{\omega}(x_2 + x_3 - 1)(4\hat{m}_b(x_2 + x_3 - 1) \\ & - 3x_2 - 3x_3 + 4) - 2(\hat{m}_b - 1)(x_3 - 1)(x_2 + x_3)) - m_B^4 (\hat{\omega}(x_2 + x_3 - 1) \\ & - x_3 + 1) \left(3(2\hat{m}_b - 1)\hat{\omega}^2(x_2 + x_3 - 1)^2(x_2 + x_3) - \hat{\omega}(x_2 + x_3 - 1)(x_2(8\hat{m}_b x_3 \right. \\ & - 2\hat{m}_b - 5x_3 + 2) + x_3(8\hat{m}_b x_3 - 2\hat{m}_b - 5x_3 + 3)) + 2(\hat{m}_b - 1)(x_3 - 1)x_3(x_2 + x_3) \left. \right) \\ & \left. - (x_3 - 1)x_3 s^2 (\hat{\omega}(x_2 + x_3 - 1) - x_3 + 1)(4\hat{m}_b(x_2 - 1)\hat{\omega} + (4\hat{m}_b - 1)x_3(\hat{\omega} - 1) - x_2\hat{\omega}) \right), \end{aligned}$$

$$\begin{aligned} D_1^{(4,\phi)}(s, q^2) = & -4 \left(-s \left(\hat{m}_b \hat{\omega} (2x_2(8x_3 - 5) + 2x_3(8x_3 - 13) + 11) - 2\hat{m}_b(x_3(8x_3 - 9) + 4) \right. \right. \\ & + \hat{\omega}^2(x_2 + x_3 - 2)(x_2 + x_3 - 1) + x_3 \hat{\omega} (-6x_2 - 6x_3 + 5) + 3(x_2 - 1)\hat{\omega} \\ & + x_3(5x_3 - 4) + 2) + q^2 \left(\hat{\omega} (\hat{m}_b (2x_2(8x_3 - 5) + 2x_3(8x_3 - 13) + 11) \right. \\ & - 12x_3(x_2 + x_3) + 9x_2 + 23x_3 - 9) - 2(\hat{m}_b - 1)(x_3 - 1)(3x_3 - 2) + \hat{\omega}^2(x_2 \\ & + x_3 - 2)(x_2 + x_3 - 1) \left. \right) + 2\hat{\omega}^2(x_2 + x_3 - 1) \left(m_B^2 (\hat{m}_b(11x_2 + 11x_3 - 8) \right. \\ & - 5x_2 - 5x_3 + 3) + 2(8\hat{m}_b(x_2 + x_3 - 1) - 5x_2 - 5x_3 + 6) \left. \right) + \hat{\omega} \left(m_B^2 (\hat{m}_b(x_2(18 \right. \\ & - 28x_3) + 4(10 - 7x_3)x_3 - 17) + 16x_3(x_2 + x_3) - 11x_2 - 28x_3 + 11) \\ & + 2(-2\hat{m}_b(2x_2(5x_3 - 3) + 2x_3(5x_3 - 7) + 5) + 13x_3(x_2 + x_3) - 8x_2 - 19x_3 + 8) \left. \right) \\ & \left. + 2(x_3 - 1)(m_B^2 (\hat{m}_b - 1)(3x_3 - 2) + 6\hat{m}_b x_3 - 4x_3) \right), \end{aligned}$$

$$D_2^{(4,\phi)}(s, q^2) = -12(2\hat{m}_b - 1).$$

E.3 Coefficients $F_n^{(X)}$

The coefficients used in the $I^{(D1)}$ function are given below:

$$F_1^{(\Psi_{AV})}(q^2, \omega) = \frac{3}{m_b^2}(1 - \hat{\omega})m_B(2\hat{m}_b - 1), \quad F_2^{(\Psi_{VA})}(q^2, \omega) = 0,$$

$$F_1^{(\Psi_V)}(q^2, \omega) = \frac{6}{m_b^2}(1 - \hat{\omega})m_B(2\hat{m}_b - 1), \quad F_2^{(\Psi_V)}(q^2, \omega) = 0,$$

$$F_1^{(X_A)}(q^2, \omega) = -\frac{2}{m_b^2}(1 - 2\hat{m}_b), \quad F_2^{(X_A)}(q^2, \omega) = -\frac{1}{m_b^2}(1 - 2\hat{m}_b)((1 - \hat{\omega})^2 m_B^2 - q^2),$$

$$F_1^{(W_{YA})}(q^2, \omega) = \frac{-4}{(1 - \hat{\omega})^2 m_B^2}, \quad F_2^{(W_{YA})}(q^2, \omega) = \frac{4((1 - \hat{\omega})^3 m_B^2 + q^2(2\hat{\omega} - 1))}{(1 - \hat{\omega})^2 m_B^2},$$

$$F_1^{(\tilde{X}_A)}(q^2, \omega) = F_1^{(X_A)}(q^2, \omega), \quad F_2^{(\tilde{X}_A)}(q^2, \omega) = F_2^{(X_A)}(q^2, \omega),$$

$$F_1^{(\tilde{Y}_A)}(q^2, \omega) = F_1^{(W_{YA})}(q^2, \omega), \quad F_2^{(\tilde{Y}_A)}(q^2, \omega) = F_2^{(W_{YA})}(q^2, \omega).$$

We compared our results for these diagrams with the ones obtained earlier in [7] and found a full agreement between expressions (up to certain twist-3 DAs that were not included yet in that computation). The only difference is in the coefficient $F_1^{(X_A)}(q^2, \omega)$, which, according to [7] is equal to $\frac{-1}{m_b^2}(2 + \hat{m}_b)$.

References

- [1] CMS collaboration, *Test of lepton flavor universality in $B^\pm \rightarrow K^\pm \mu^+ \mu^-$ and $B^\pm \rightarrow K^\pm e^+ e^-$ decays in proton-proton collisions at $\sqrt{s} = 13$ TeV*, *Rept. Prog. Phys.* **87** (2024) 077802 [2401.07090].
- [2] LHCb collaboration, *Differential branching fractions and isospin asymmetries of $B \rightarrow K^{(*)} \mu^+ \mu^-$ decays*, *JHEP* **06** (2014) 133 [1403.8044].
- [3] T. Hurth, F. Mahmoudi, Y. Monceaux and S. Neshatpour, *Data-driven analyses and model-independent fits for present $b \rightarrow s \ell \ell$ results*, 2508.09986.
- [4] R. Frezzotti, G. Gagliardi, V. Lubicz, G. Martinelli, C.T. Sachrajda, F. Sanfilippo et al., *Theoretical framework for lattice QCD computations of $B \rightarrow K \ell^+ \ell^-$ and $\bar{B}_s \rightarrow \ell^+ \ell^- \gamma$ decays rates, including contributions from "Charming Penguins"*, 2508.03655.
- [5] M. Beneke, T. Feldmann and D. Seidel, *Systematic approach to exclusive $B \rightarrow V \ell^+ \ell^-$, $V \gamma$ decays*, *Nucl. Phys. B* **612** (2001) 25 [hep-ph/0106067].
- [6] A. Khodjamirian, T. Mannel, A.A. Pivovarov and Y.M. Wang, *Charm-loop effect in $B \rightarrow K^{(*)} \ell^+ \ell^-$ and $B \rightarrow K^* \gamma$* , *JHEP* **09** (2010) 089 [1006.4945].
- [7] A. Khodjamirian, T. Mannel and Y.M. Wang, *$B \rightarrow K \ell^+ \ell^-$ decay at large hadronic recoil*, *JHEP* **02** (2013) 010 [1211.0234].

- [8] A. Khodjamirian and A.V. Rusov, $B_s \rightarrow K \ell \nu_\ell$ and $B_{(s)} \rightarrow \pi(K) \ell^+ \ell^-$ decays at large recoil and CKM matrix elements, *JHEP* **08** (2017) 112 [1703.04765].
- [9] C. Bobeth, M. Chrzaszcz, D. van Dyk and J. Virto, Long-distance effects in $B \rightarrow K^* \ell \ell$ from analyticity, *Eur. Phys. J. C* **78** (2018) 451 [1707.07305].
- [10] N. Gubernari, D. van Dyk and J. Virto, Non-local matrix elements in $B_{(s)} \rightarrow \{K^{(*)}, \phi\} \ell^+ \ell^-$, *JHEP* **02** (2021) 088 [2011.09813].
- [11] N. Gubernari, M. Reboud, D. van Dyk and J. Virto, Improved theory predictions and global analysis of exclusive $b \rightarrow s \mu^+ \mu^-$ processes, *JHEP* **09** (2022) 133 [2206.03797].
- [12] A. Khodjamirian, T. Mannel and N. Offen, Form-factors from light-cone sum rules with B -meson distribution amplitudes, *Phys. Rev. D* **75** (2007) 054013 [hep-ph/0611193].
- [13] F. De Fazio, T. Feldmann and T. Hurth, Light-cone sum rules in soft-collinear effective theory, *Nucl. Phys. B* **733** (2006) 1 [hep-ph/0504088].
- [14] A. Khodjamirian, B. Melić and Y.-M. Wang, A guide to the QCD light-cone sum rules for b -quark decays, *Eur. Phys. J. ST* **233** (2024) 271 [2311.08700].
- [15] V.M. Braun, Y. Ji and A.N. Manashov, Higher-twist B -meson Distribution Amplitudes in HQET, *JHEP* **05** (2017) 022 [1703.02446].
- [16] M. Bordone, A. Khodjamirian and T. Mannel, New sum rules for the $B_c \rightarrow J/\psi$ form factors, *JHEP* **01** (2023) 032 [2209.08851].
- [17] H.H. Asatryan, H.M. Asatrian, C. Greub and M. Walker, Calculation of two loop virtual corrections to $b \rightarrow s l^+ l^-$ in the standard model, *Phys. Rev. D* **65** (2002) 074004 [hep-ph/0109140].
- [18] V.M. Braun, D.Y. Ivanov and G.P. Korchemsky, The B meson distribution amplitude in QCD, *Phys. Rev. D* **69** (2004) 034014 [hep-ph/0309330].
- [19] A. Khodjamirian, R. Mandal and T. Mannel, Inverse moment of the B_s -meson distribution amplitude from QCD sum rule, *JHEP* **10** (2020) 043 [2008.03935].
- [20] T. Nishikawa and K. Tanaka, QCD Sum Rules for Quark-Gluon Three-Body Components in the B Meson, *Nucl. Phys. B* **879** (2014) 110 [1109.6786].
- [21] M. Rahimi and M. Wald, QCD sum rules for parameters of the B -meson distribution amplitudes, *Phys. Rev. D* **104** (2021) 016027 [2012.12165].
- [22] A. Khodjamirian, T. Mannel and M. Melcher, Flavor $SU(3)$ symmetry in charmless B decays, *Phys. Rev. D* **68** (2003) 114007 [hep-ph/0308297].
- [23] N. Gubernari, A. Kokulu and D. van Dyk, $B \rightarrow P$ and $B \rightarrow V$ Form Factors from B -Meson Light-Cone Sum Rules beyond Leading Twist, *JHEP* **01** (2019) 150 [1811.00983].
- [24] PARTICLE DATA GROUP collaboration, Review of particle physics, *Phys. Rev. D* **110** (2024) 030001.
- [25] FLAVOUR LATTICE AVERAGING GROUP (FLAG) collaboration, FLAG Review 2024, 2411.04268.

- [26] F. Mahmoudi, *SuperIso v2.3: A Program for calculating flavor physics observables in Supersymmetry*, *Comput. Phys. Commun.* **180** (2009) 1579 [0808.3144].
- [27] M.L. Piscopo and A.V. Rusov, *Non-factorisable effects in the decays $\overline{B}_s^0 \rightarrow D_s^+ \pi^-$ and $\overline{B}^0 \rightarrow D^+ K^-$ from LCSR*, *JHEP* **10** (2023) 180 [2307.07594].
- [28] B. Grinstein, M.J. Savage and M.B. Wise, *$B \rightarrow X_s e^+ e^-$ in the Six Quark Model*, *Nucl. Phys. B* **319** (1989) 271.
- [29] M. Misiak, *The $b \rightarrow se^+e^-$ and $b \rightarrow s\gamma$ decays with next-to-leading logarithmic QCD corrections*, *Nucl. Phys. B* **393** (1993) 23.
- [30] A.J. Buras and M. Munz, *Effective Hamiltonian for $B \rightarrow X_s e^+ e^-$ beyond leading logarithms in the NDR and HV schemes*, *Phys. Rev. D* **52** (1995) 186 [hep-ph/9501281].
- [31] G. Buchalla, A.J. Buras and M.E. Lautenbacher, *Weak decays beyond leading logarithms*, *Rev. Mod. Phys.* **68** (1996) 1125 [hep-ph/9512380].
- [32] M. Beneke, V.M. Braun, Y. Ji and Y.-B. Wei, *Radiative leptonic decay $B \rightarrow \gamma \ell \nu_\ell$ with subleading power corrections*, *JHEP* **07** (2018) 154 [1804.04962].
- [33] A.G. Grozin and M. Neubert, *Asymptotics of heavy meson form-factors*, *Phys. Rev. D* **55** (1997) 272 [hep-ph/9607366].